Journal of Japan Association for Earthquake Engineering, Vol. 20, No. 5, 2020

STATIC DISPLACEMENT AND LONG-PERIOD VELOCITY PULSE OF CRUSTAL EARTHQUAKES IN JAPAN

Toshimi SATOH[1]

[1] Member, Research Fellow, Institute of Technology, Shimizu Corporation,
Tokyo, Japan, toshimi.satoh@shimz.co.jp

ABSTRACT: We extract static displacement D_p and long-period (2–10 s) velocity pulse from strong motion records of crustal earthquakes in Japan and examine them by comparing with those of the 2016 Kumamoto earthquake and previous prediction equations. The period of long-period pulse of four earthquakes with Mw6.6–Mw7.0 is about 3 s, which is consistent to one of previous equations. Prediction of D_p is improved by substituting the relation between seismic moment and rupture area derived in this study using fault models from geodetic data into the equation by Kamai et al. (2014).

Keywords: Static displacement, Long-period velocity pulse, Crustal earthquake, Scaling relation

1. INTRODUCTION

During the 2016 Kumamoto earthquake with Japan Meteorological Agency magnitude (M_J) 7.3 surface ruptures were widely exposed. Displacement time histories integrated from many acceleration records observed at near-fault regions including Nishihara strong motion station[e.g.1),2)] contained fling-steps. The static displacement of the maximum direction (we call as “Fling-P component” which means the parallel direction to the fling-step) of the horizontal vector was 154 cm and that of vertical component was 179 cm at Nishihara[2)]. Long-period velocity pulses with periods of a little less than 3 s were contained in the velocity time histories at Nishihara[2)], and the peak ground velocities (PGVs) of the Fling-P component and vertical component were 277 cm/s and 152 cm/s, respectively. At the other several stations static displacements and PGVs of Fling-P components were around 100 cm and larger than 100 cm/s. These static displacements are larger than clearances of ordinary base-isolation buildings and probably lead to deformations of buildings with natural periods longer than the velocity pulses. Long-period velocity pulses may influence on long-period structures such as super high-rise buildings and base-isolated buildings.

During the 2008 Iwate-Miyagi Nairiku earthquake static displacements of 50 cm for horizontal components and 150 cm for the vertical component were observed at Ichinosekinishi strong motion station (IWTH25)[3),4)]. Surface ruptures were exposed during the 2008 Iwate-Miyagi Nairiku earthquake[5)], the 2004 Niigata-ken Chuetsu earthquake[6)], 2011 Fukushima-ken Hamadori earthquake[7)] and the 2014 Nagano-ken Hokubu earthquake[8)]. Crustal deformations were observed at GNSS stations by Geospatial Information Authority of Japan[9)], but post-seismic deformations were sometimes contaminated in the GNSS data. Additionally, the number of GNSS stations in near-fault regions was small and the sampling-rate of ordinary GNSS data at in Japan is longer than 1 s and so the GNSS data are not enough to estimate the velocity pulse of about 2 s. Since a dense strong motion network has been deployed, static displacements and long-period velocity pulses could be extracted from the strong motion records in near-fault regions.

In this study we extract static displacements and long-period velocity pulses from strong motion records of crustal earthquakes in Japan. We examine them including those of the 2016 Kumamoto earthquake studied in our paper[2)] by comparing with previous prediction equations. The previous prediction equations[10)–13)] of periods of long-period velocity pulses due to fling-steps have been modeled using a moment magnitude Mw. Abrahamson[10),11)] developed a prediction equation from strong motion records of three earthquakes outside of Japan with Mw larger than 7.3. Kamai et al.[12)] developed a prediction equation from synthetics ground motions. Burks and Baker[13)] developed a prediction equation from observed and synthetic ground motions, but strong motion records in Japan were only for the 2003 Tokachi-oki earthquake which was an interplate earthquake. In previous prediction equations of static displacements, no strong motion records of crustal earthquakes in Japan were used. The strong motion prediction method used to synthesize ground motions was different from that ordinary used in Japan so-called “Recipe”[17),18)]. In the prediction equations by Kamai et al.[12)] and Burks and Baker[13)] ground motions synthesized using the relation between seismic moment M_0 and rupture area S by Wells and Coppersmith[19)]. In this study we estimate an M_0–S relation from crustal earthquakes in Japan and discuss the prediction equation using the estimated M_0–S relation, instead of that by Wells and Coppersmith[19)].

We are aiming for the development of empirical prediction equations of static displacements and the periods of long-period velocity pulses using worldwide strong motion records of crustal earthquakes. In this study we analyze static displacements and long-period velocity pulses using strong motion records of crustal earthquakes in Japan as the first step. After the 2016 Kumamoto earthquake, studies on extension of “Recipe” for long-period strong motions of surface rupture earthquakes were carried out[e.g.20)]. Validation of predicted strong motions by empirical prediction equations is required in “Recipe” [18)], so this study will contribute to improvement of strong motion predictions of surface rupture earthquakes.

2. DATA AND METHOD

We select strong motion records of four surface rupture earthquakes[5)–8)] and one Mw6.7 buried rupture earthquake from records after the 1995 Hyogo-ken Nanbu earthquake in Japan. The five earthquakes are listed in Table 1[21)–28)]. Since we analyze static displacements and long-period velocity pulses due to fling-steps, fault models estimated from geodetic data[21)–25)] shown in Table 1 are used for the comparison with previous equations.

Strong motion records of K-NET[29),30)], KiK-net[30)], JMA[31)], local governments[31)], National Institute for Land, Infrastructure Management[32),33)], NEXCO East and JR East are used. Data of NEXCO East and JR East are given from Japan Society of Civil Engineers[34)] download site. Records with rupture distance R_{rup} less than 30 km are selected for analyses.

Table 1 List of earthquakes

Event	M_J	Fault Models from Geodetic Data						Hypocenter
		Reference	Fault Type	M_0[Nm]	Mw	Number of Faults	Top Depth of Fault Z_{TOR}[km]	Reference
2000 Tottori-ken Seibu earthquake	7.3	Sagiya et al[21)]	Strike-slip	1.36E+19	6.7	10	1.00	JMA
2004 Niigata-ken Chuetsu earthquake	6.8	GSI[22)]	Reverse-slip	1.15E+19	6.6	1	2.80	26)
2008 Iwate-Miyagi Nairiku earthquake	7.2	Ohta et al.[23)]	Reverse-slip	2.70E+19	6.9	2	0.46, 0.40	27)
2011 Fukushima-ken Hamadori earthquake	7.0	Kabayashi et al.[24)]	Reverse-slip	1.45E+19	6.7	2	0.00	JMA
2014 Nagano-ken Hokubu earthquake	6.7	GSI[25)]	Reverse-slip	2.68E+18	6.2	1	0.14	28)

In Fig. 1, the static displacement D_p and the period T_p of velocity pulse of the horizontal component estimated in this study are shown together with fault models[21)–25)], epicenters[26)–28)], F-net mechanisms[35)] and crustal deformations by GNSS. For the 2004 Niigata-ken Chuetsu earthquake and the 2008 Iwate-Miyagi Nairiku earthquake, those of vertical component are also shown in Fig. 1. For the 2014 Nagano-ken Hokubu earthquake D_p of vertical component at NGN005 (Hakuba) is estimated to be 11 cm. D_p estimated from strong motion records of Fling-P and vertical components larger than 10 cm and 5 cm, respectively[2)] are used in this study. Strong motion time histories and the 5%-damped velocity response spectra at stations with station names in Fig. 1 will be shown later. Four-digit number for the government seismic intensity meter and the first six-digit number for the JMA seismic intensity meter are shown as station names. Borehole records of KiK-net stations are named putting B at the end. NCOIDE (Koide), NECIGO (Echigokawaguchi) and NICHIK (Ichinoseki) were observed

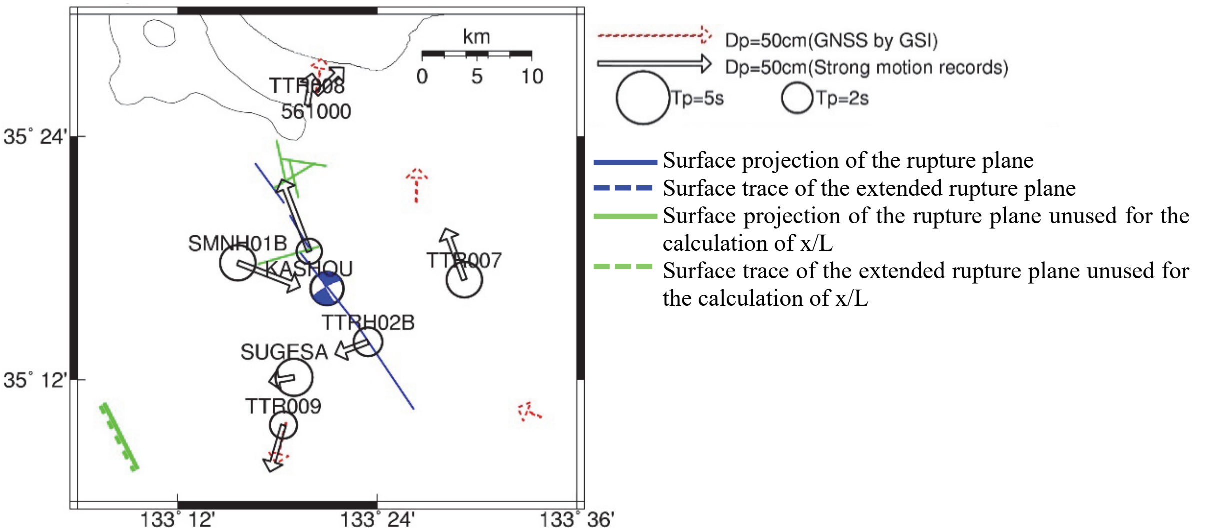

(a) 2000 Tottori-ken Seibu earthquake
(Fling-P component)

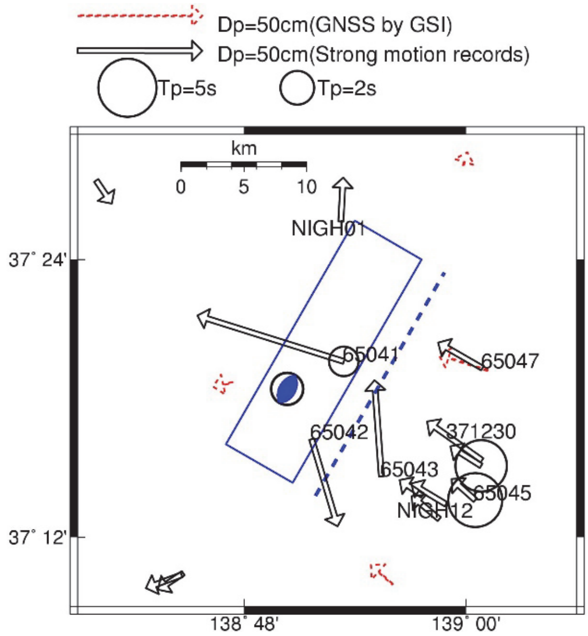

(b) 2004 Niigata-ken Chuetsu earthquake
(Fling-P component)

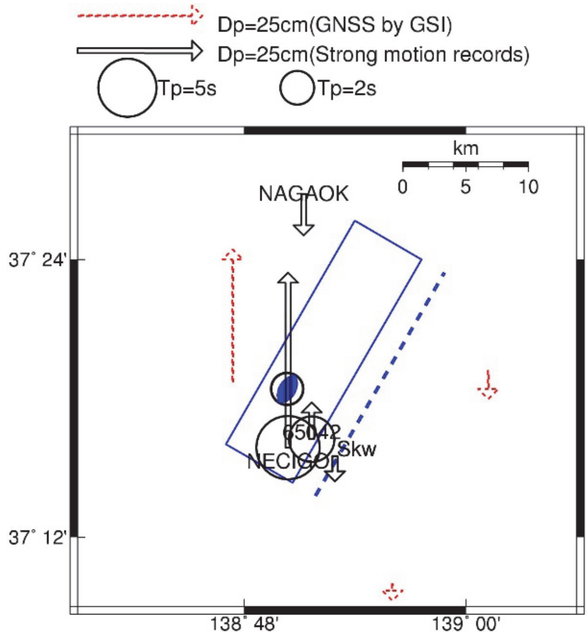

(c) 2004 Niigata-ken Chuetsu earthquake
(Vertical component)

Fig. 1 Static displacement D_p and the period T_p of velocity pulse extracted in this study together with fault models, epicenters, F-net mechanisms and crustal deformations by GNSS

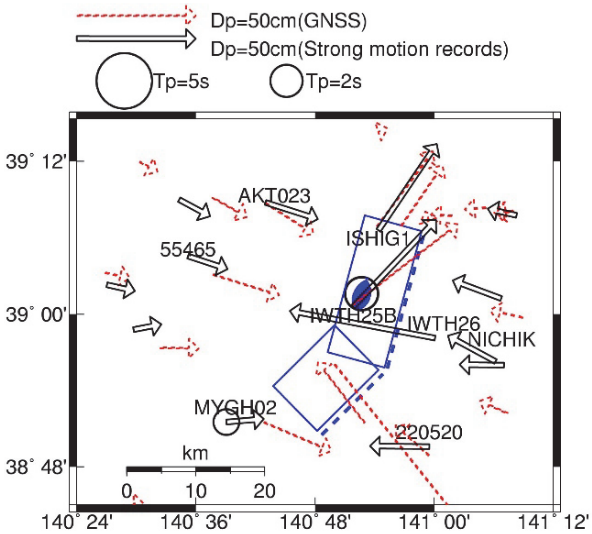

(d) 2008 Iwate-Miyagi Nairiku earthquake
(Fling-P component)

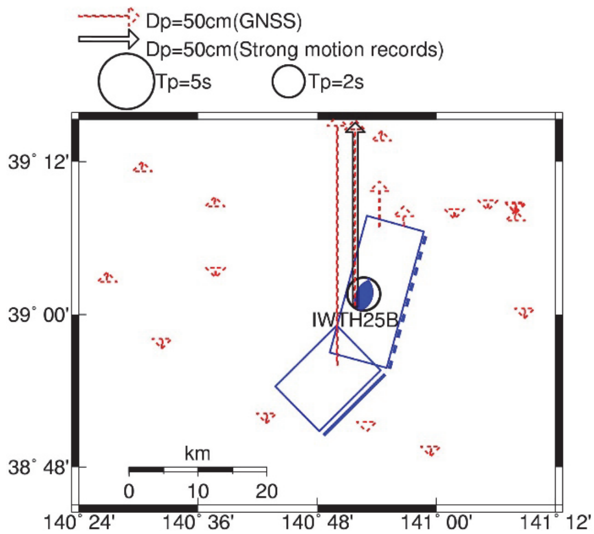

(e) 2008 Iwate-Miyagi Nairiku earthquake
(Vertical component)

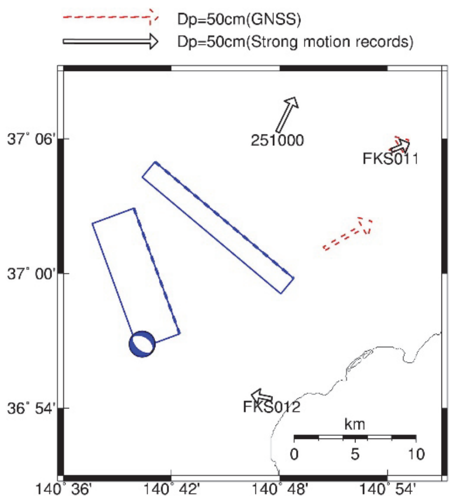

(f) 2011 Fukushima-ken Hamadori earthquake
(Fling-P component)

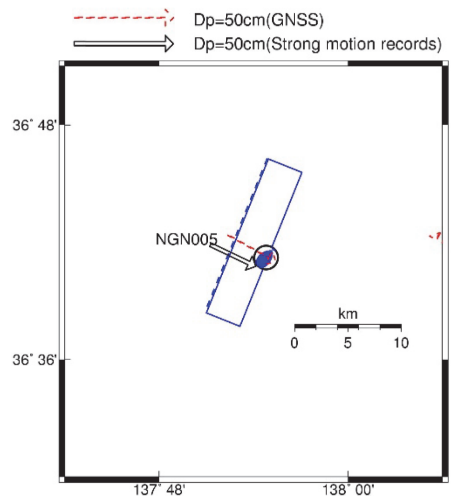

(g) 2014 Nagano-ken Hokubu earthquake
(Fling-P component)

Fig. 1 Continued

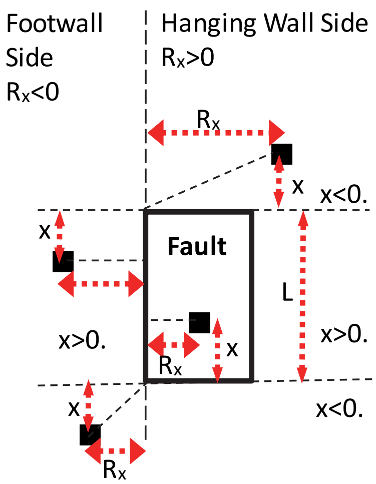

(a) Plan view

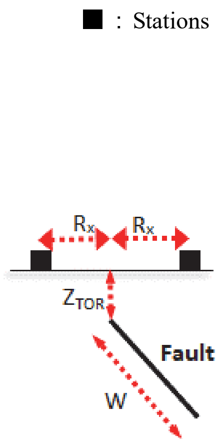

(b) Cross-section view

Fig. 2 Schematic view added to 2) of parameters used in previous prediction equations by NEXCO East[34]. NAGAOKA (Nagaoka) and Skw (Shinkawaguchi) were observed by JR East[34]. Strong motion records at dam sites[32),33] were observed in inspection gallery at KASHOU (Kasyo dam), the lower inspection gallery at SUGESA (Sugesawa dam) and the right bank at ISHIG1 (Ishibuchi dam). The crustal deformations by GNSS were estimated by Geospatial Information Authority of Japan[9] except for data of the 2008 Iwate-Miyagi Nairiku earthquake by Ohta et al.[23].

Most of D_p estimated in this study are consistent with D_p by GNSS close to the strong motion station, but some of D_p are not. The causes of the difference are the contamination of post-seismic deformation to D_p by GNSS and the accuracy of D_p estimated in this study. In fact, many large aftershocks occurred successively after the 2004 Niigata-ken Chuetsu earthquake, so crustal deformations by the aftershocks as well as post-seismic deformations were observed by GNSS[22]. The fault models in Table 1 are homogeneous slip models[22)–25] except for the heterogeneous slip-model for the 2000 Tottori-ken Seibu earthquake[21]. A few D_p by GNSS were not simulated well by homogeneous slip models. Ohta et al.[23] pointed out that the cause of the poor simulation was the assumption of homogeneous slips. For this reason, in this study, D_p estimated from strong motion records is not compared with D_p calculated from fault models.

We estimate D_p from strong motion records observed by JMA[31], CEORKA[36),37] and Architectural Institute of Japan[38] for the 1995 Hyogo-ken Nanbu earthquake, but there are no records with D_p larger than 10 cm for Fling-P components and 5 cm for vertical components. It is thought that there were no strong motion stations near the Nojima fault where surface ruptures were exposed and that strong motion stations in Kobe city were located on the foot-wall side where horizontal crustal deformations estimated from geodetic data were less than 10 cm[39].

D_p and long-period velocity pulses are estimated by the same method as Satoh[2]. The method[2] is as follows. After the zero-line correction to acceleration records, trends of the integrated velocity time histories are removed by the method by Zahradník and Plešinger[40] and then displacement time histories are integrated form the corrected velocity time histories. The analyzed duration starts from 60 s after the origin time and is shortened by each 5 s to get stable D_p. The minimum analyzed duration is 20 s. D_p is the average value from 20 s to the end after the origin time. In the case of the analyzed duration of 20 s, D_p is the average value from 15 s to 20 s. Data without stable D_p are removed. Velocity and displacement time histories at IWTH25B (at a depth of 260 m at Ichinosekinishi) by Satoh[4] are used in this study. All horizontal components rotate to Fling-P and Fling-N components. Here Fling-N components mean the orthogonal components to Fling-P components. No filters apply to time histories. We define long-period pulses by following conditions. One is that the period of the maximum peak of 5%-damped velocity response spectrum Sv between 1 s and 10 s is longer than 2 s. The other is that the maximum velocity V_{max} occurs within duration of fling-steps. We call the period of the long-period pulse as T_p[2]. Here duration of the fling-step is visually identified from each displacement time history. Since static displacements in Fling-N components are zero and so there are no long-period pulses, we will not analyze Fling-N components except for the Sv to use for the examination of the effects of site amplifications on long-period pulses of Fling-P components.

The long-period pulse $V_f(t)$ is modeled by Eq. (1)[2].

$$V_f(t) = V_{max}/2(1 - \cos(2\pi/T_p(t - t_1))) \qquad \text{for } t_1 \le t \le t_1 + T_p \quad (1)$$

where t [s] is the time from the origin time, $V_f(t)$ is zero in $t < t_1$ and $t > t + T_p$. Equation (1) is defined by replacing D_p/T_p in an equation by Kamai et al.[12] with $V_{max}/2$ considering the sign. The value t_1 is estimated by a nonlinear least-squares method by using $t_{max} - T_p/4$ as an initial value where t_{max} is the occurrence time of V_{max}.

Figure 2 illustrates definitions[41] of R_x, x, L, W and Z_{TOR} which are used for the comparison of D_p and T_p estimated in this study with previous prediction equations. In the case of several faults, R_x is calculated from the fault with the shortest R_{rup}. The x/L for the 2000 Tottori-ken Seibu earthquake is calculated from faults denoted by blue lines shown in Fig. 1(a).

3. STATIC DISPLACEMENTS AND LONG-PERIOD PULSES ESTIMATED FROM STRONG MOTION RECORDS

Figure 3 shows Sv and T_p of Fling-P and Fling-N components, and velocity and displacement time histories of Fling-P components for three earthquakes in which T_p is identified. The azimuths of Fling-P components are also shown in Fig. 3. The value upper right of each time history is peak

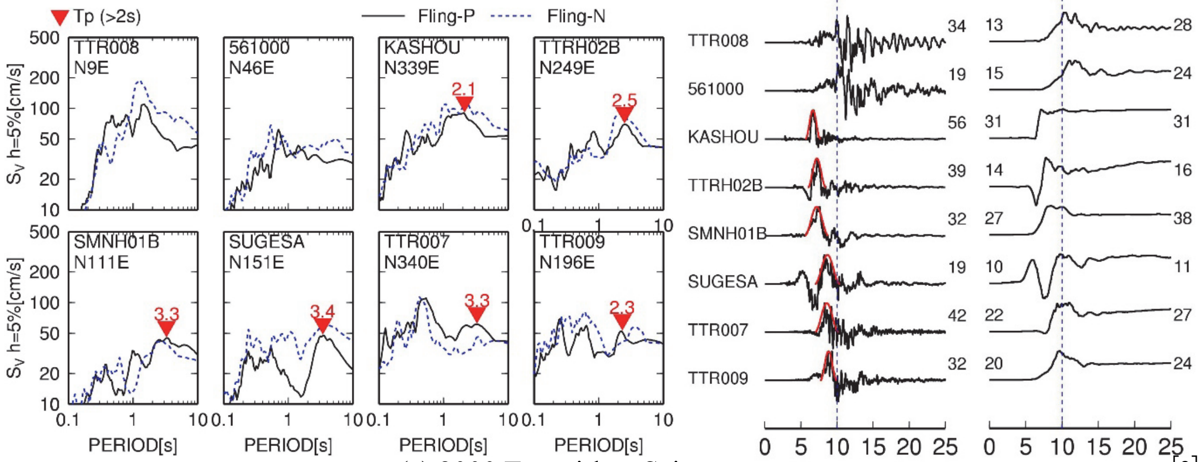

(a) 2000 Tottori-ken Seibu earthquake

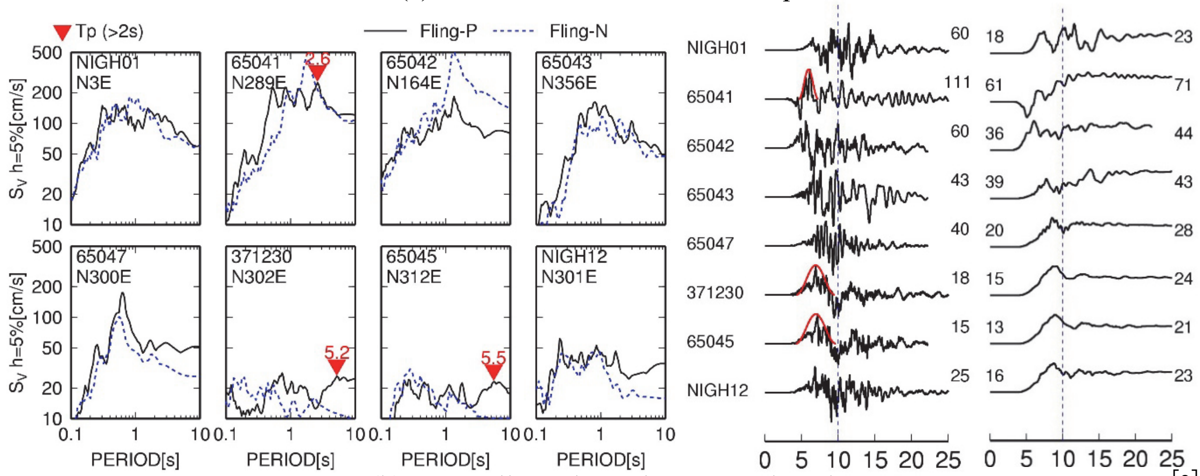

(b) 2004 Niigata-ken Chuetsu earthquake

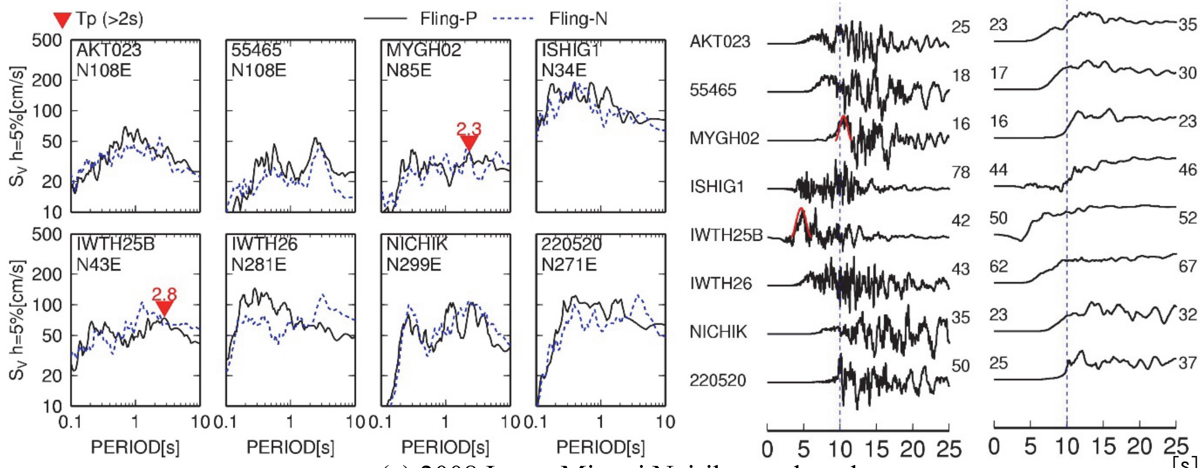

(c) 2008 Iwate-Miyagi Nairiku earthquake

Fig. 3 Sv and T_p of Fling-P and Fling-N components (left figures), velocity (middle figures) and displacement (right figures) time histories of Fling-P components ground velocity PGV [cm/s] or peak ground displacement PGD [cm]. The value left of each displacement time history is D_p [cm]. Dotted lines are plotted at 10 s to make it easy to see the occurrence time of long-period pulses and fling-steps.

For the 2000 Tottori-ken Seibu earthquake D_p larger than 10 cm is identified at eight stations and T_p is obtained at six stations out of eight stations. Two stations are dam sites and the other two stations are KiK-net borehole stations. *V*s30 derived from the empirical relation by Midorikawa and Nogi[42] using PS loggings in the top 20 m is 553 m/s at TTR007 and 521 m/s at TTR009. The amplification factors[43] at both stations are nearly one at periods longer than 2 s. It is thought from these results that 3 s pulses are generated from the source. The fling-step direction at KASHOU (Kasyo dam) located in the very near-fault is parallel to the fault and the velocity time history contains a typical one-sided pulse. Fling-steps and long-period pulses at SMNH01B (a depth of 101 m at Hakuta) and TTRH02B (a depth of 100 m at Hino) in the very near-fault are noticeable. SMNH01B is located near the edge of the right-lateral strike-slip fault with east–west strike direction. Fling-P direction observed at SMNH01B is consistent with the theoretical direction estimated by Okada's method[44),45]. Fling-P direction observed at TTRH02B is almost normal to the closest fault and is the same to Fling-P direction observed at SUGESA (Sugesawa dam). A west dipping fault was estimated in some fault models[46),47] instead of the vertical fault near TTRH02B, but it is unknown if the direction can be simulated using the west dipping fault because the record at TTRH02B was not used for the source inversions. The *S*v at T_p of Fling-P components at six stations except for TTR007 are equal or smaller than those of Fling-N components. It is thought that rupture directivity influences on fault normal components. D_p in Fig. 3(a) is less than 40 cm, that is, less than half of D_p observed at near-fault stations during the 2016 Kumamoto earthquake.

For the 2004 Niigata-ken Chuetsu earthquake, D_p larger than 10 cm is identified at 14 stations and T_p is obtained at three stations out of 14 stations. *S*v at T_p of Fling-P components on the foot-wall stations, 65045 (Yunotani) and 371230 (Hirokami) is larger than that of Fling-N components, but the absolute *S*v is small. Peaks in Fling-P components at 65045 (Yunotani) and 371230 (Hirokami) are not caused by site amplifications, because no peaks are shown in the Fling-N components. The amplitude of *S*v at T_p of Fling-P component at 65041 (Yamakoshi) is the same to that of the Fling-N component. In order to examine the effects of site amplifications at T_p of 2.6 s at 650418 (Yamakoshi), Fig. 4 shows the distance-corrected spectra at 650418 (Yamakoshi), 65042 (Kawaguchi) and NIGH12 (Yunotani) with respect to a spectrum at NIGH12B (a depth of 110 m at Yunotani) during the 2007 Niigata-ken Chuetsu-oki earthquake. Geometric attenuation and the frequency *f* dependent Q (= 30f) are used for the distance-correction to geometric mean spectra of horizontal components. Peak ground accelerations of horizontal components are also shown in Fig.4. The other earthquakes proper to the analysis were not observed at 650418 (Yamakoshi), because only strong motion records with large amplitudes were open in public. The empirical amplification factors at NIGH12 (Yunotani) estimated by Sakai and Nozu[48] were about two at periods shorter than 1 s. These results mean that the peak at 2.6 s at 65041 (Yamakoshi) in Fig. 3(b) is not caused by the site amplification. Since 65041 (Yamakoshi) and 65042 (Kawaguchi town hall) are located at the forward direction from the rupture initiation point, amplifications at about 1 s are influenced by the rupture directivity. The direction of Fling-P component at 65041 (Yamakoshi) is not consistent with the direction on the hanging-wall side

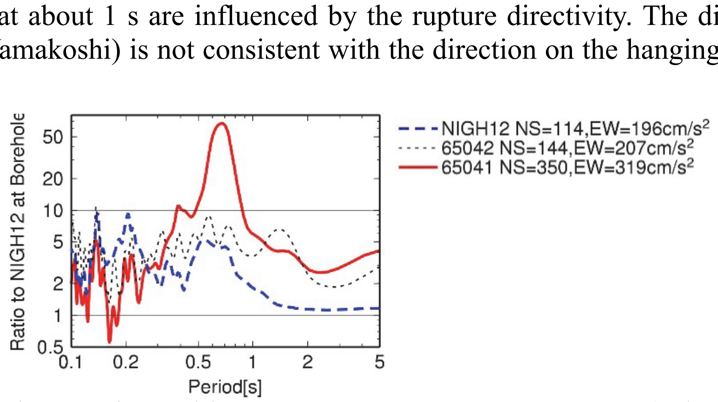

Fig. 4 Fourier spectral ratios at three stations with respect to a spectrum at NIGH12B (a depth of 110 m at Yunotani) during the 2007 Niigata-ken Chuetsu-oki earthquake (Horizontal component)

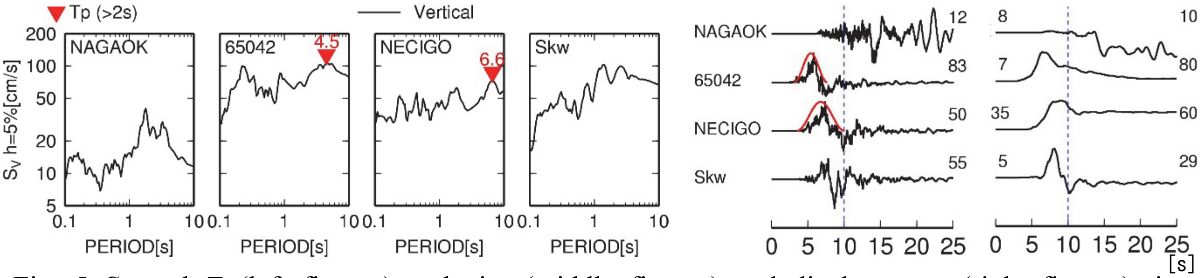

Fig. 5 *S*v and T_p (left figures), velocity (middle figures) and displacement (right figures) time histories of vertical component for the 2004 Niigata-ken Chuetsu earthquake

for reverse faults. The direction of the initial part of the displacement is the inverse direction to the static displacement and this feature is the same to that of displacement time history at TTRH02B (a depth of 100 m at Hino) of the 2000 Tottori-ken Seibu earthquake. Since 65041 (Yamakoshi) is located at the top edge of the hanging-wall side, the record is probably affected by complex ground motions. D_p of vertical component at 65041 (Yamakoshi) is estimated to be almost zero.

For the 2008 Iwate-Miyagi Nairiku earthquake, T_p is obtained only at IWTH25B (a depth of 260 m at Ichinosekinishi) and MYGH02 (Naruko). *S*v at T_p of Fling-P component is the same level to that of Fling-N component at both stations. MYGH02 (Naruko) is in x < 0 km which is outside of the prediction equations of T_p and D_p by Kamai et al.[12)].

No long-period pulses are identified form records of the 2011 Fukushima-ken Hamadori earthquake, although D_p of 10 to 20 cm are estimated from Fling-P components at three stations shown in Fig. 1(f). No long-period pulses are also identified form the records of the 2014 Nagano-ken Hokubu earthquake, although D_p of 27 cm is estimated from Fling-P component at NGN005 (Hakuba) shown in Fig. 1(g).

From vertical components T_p is identified only at 65042 (Kawaguchi town hall) and NECIGO (Echigokawaguchi) during the 2004 Niigata-ken Chuetsu earthquake shown in Fig. 1(c). Figure 5 shows *S*v, T_p, velocity time history and displacement time history of the vertical component at four stations during the 2004 Niigata-ken Chuetsu earthquake shown in Fig. 1(c). The meaning of numbers shown in this figure is the same to figures shown in Fig. 3. T_p at 65042 (Kawacguchi town hall) is 4.5 s and T_p at NECIGO (Echigokawaguchi) is 6.6 s, but T_p is not identified from horizontal components at the two stations. T_p of vertical components during the 2016 Kumamoto earthquake tend to be slightly longer than T_p of Fling-P components, but the difference was small compared with the data deviation. Hereafter we analyze T_p identified from the Fling-P component, since the number of T_p identified from the vertical component is small.

4. COMPARIZON WITH PREVIOUS PREDICTION EQUATIONS

T_p identified from strong motion records of three earthquakes in this study and T_p identified from strong motion records of the 2016 Kumamoto earthquake by Satoh[2)] are examined by comparing them with previous prediction equations. Figure 6 shows D_p and T_p of Fling-P components of the 2016 Kumamoto earthquake estimated by Satoh[2)] together with D_p by GNSS[9),49),50)] and the fault model with *M*w7.0 by Ozawa et al.[51)].

In Fig. 7, T_p identified in this study and Satoh[2)] is compared with prediction equations[10),12),13)]. The equation by Abrahamson[10),11)] developed from data of earthquakes with *M*w7.3–*M*w7.6 is not able to apply to earthquakes with *M*w less than 7.0 used in this study. The equation by Kamai et al.[12)] was developed from Fling-P components of 25000 synthetics for strike-slip scenarios and 25000 synthetics for reverse scenarios with x > 0. The equation by Burks and Baker[13)] was developed from observed records and synthetics of fault-parallel and fault-normal components at 100 stations with largest fling amplitude from each scenario. Kamai et al.[12)] used the synthetics calculated using fault models with the top depth of 0 km. Burks and Baker[13)] noted that their equation was basically for surface rupture earthquakes, but that some synthetics were calculated from fault models with top depths of about 5 km.

T_p identified in this study is in $|R_x| < 15$ km. It was shown by Satoh[2] that T_p in $|R_x| > 15$ km was longer than T_p in $|R_x| < 15$ km for the 2016 Kumamoto earthquake. For these reasons, T_p in $|R_x| < 15$ km is used for the comparison with the prediction equations. The distance-dependency of T_p is thought be caused by the dependency of *P*–*S* time on distance, because the static displacement by the near-field term is contained within *P*–*S* time and that by the *P* wave intermediate-term begins from *P* wave arrival. The parameter $2x/L$ (see Fig. 2) becomes maximum at the center of the rupture length and negative value outside of the rupture length. The data of $2x/L < 0$ in Fig. 7 are shown with different symbols, since the data of x < 0 km were excluded in the equation by Kamai et al.[12].

The relation between R_x and T_p for each earthquake is shown Fig. 8 to examine T_p in detail. The values of $2x/L$ are shown with different colors. T_p of the 2000 Tottori-ken Seibu earthquake with vertical strike-slip faults is plotted as $R_x > 0$ km. Most of $2x/L$ are nearly one. This result means that T_p is identified at stations near the center of the rupture length. T_p in $|R_x| < 12$ km is about 3 s except for one of the 2016 Kumamoto earthquake and is close to the equation by Burks and Baker[13]. The *M*w range from 6.6 to 7.0 is small, so that the *M*w dependency is not so clear. In the figure by Kamai et al.[12], T_p by the equation of Kamai et al. [12] was longer than T_p estimated from strong motion records of strike-slip earthquakes with *M*w7.0–*M*w7.9. Both Kami et al. [12] and Burks and Baker[13] developed the

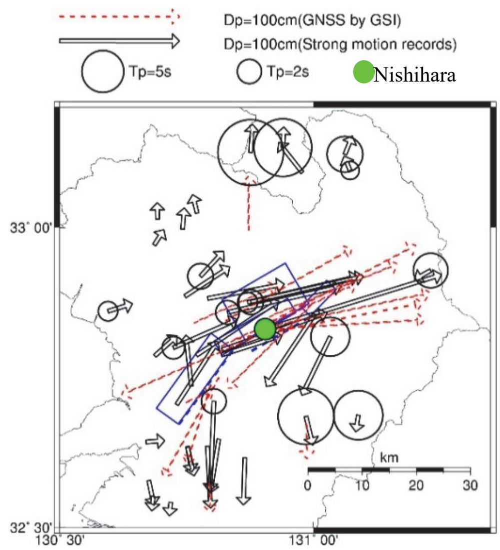

Fig. 6 D_p[2] and T_p[2] estimated from strong motion records, D_p by GNSS[9),49),50] and the fault model[51] of the 2016 Kumamoto earthquake

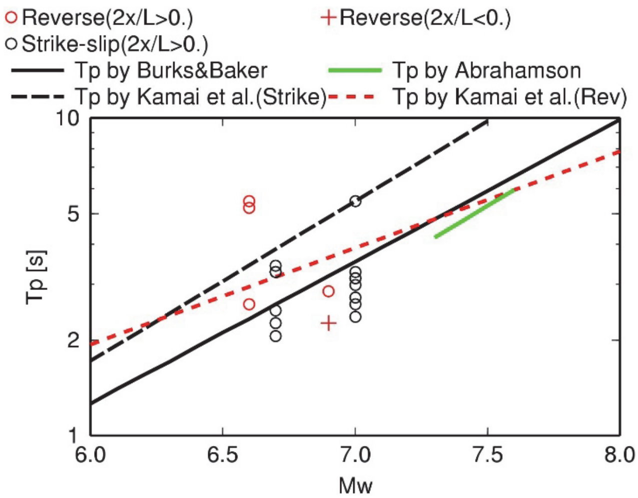

Fig. 7 Relation between M_W and T_p estimated in this study and Satoh[2] in $|R_x| < 15$ km together with the previous prediction equations[10),12),13]

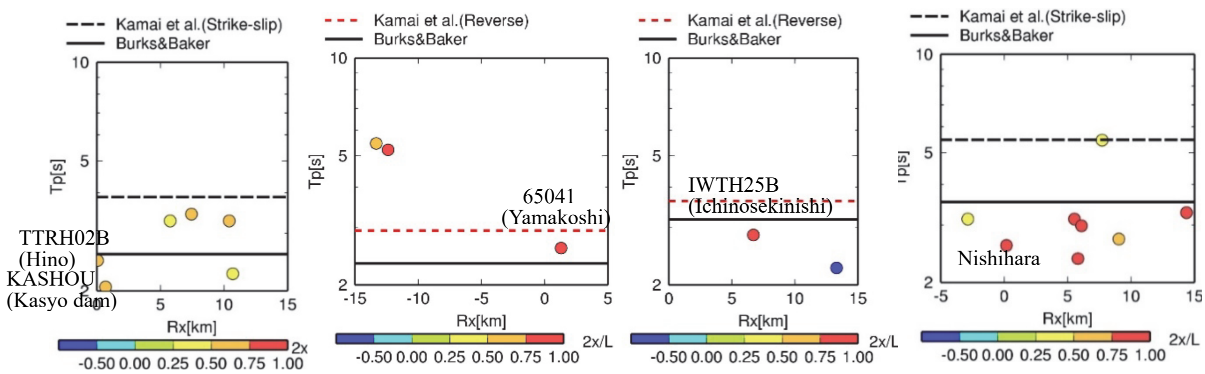

(a) Tottori-ken Seibu earthquake (b) Niigata-ken Chuetsu earthquake (c) Iwate-Miyagi Nairiku earthquake (d) Kumamoto earthquake[2]

Fig. 8 Relation between R_x and T_p estimated in this study and Satoh[2] together with the previous prediction equations

equations using data within distances of around 30 km or more which are longer than data in this study. For this reason, their T_p may be longer than T_p in this study.

The relation between D_p identified in this study and the prediction equations is examined. Dreger et al.[15] showed Eqs. (2) and (3) for D_p of the fault normal component for a vertical strike-slip fault using a depth-to-top of rupture Z_{TOR} as one of parameters.

$$D_p = \frac{D}{2}\left[1 - \tan^{-1}\left(\frac{R_x}{W}\right)\right] \qquad \text{for } Z_{TOR} = 0 \quad (2)$$

$$D_p = \frac{D}{\pi}\left[\tan^{-1}\left(\frac{R_x}{W}\right) - \frac{2}{\pi}\tan^{-1}\left(\frac{R_x}{Z_{TOR} + W}\right)\right] \qquad \text{for } Z_{TOR} > 0 \quad (3)$$

where D is an average slip. Eq. (2) is the analytical solution of an infinite vertical strike-slip fault based on dislocation theory. Dreger et al. [15] stated that the assumption of the infinite fault is reasonable in the near-fault region. Eq. (3) is the extended expression to a buried infinite fault. Dabaghi and Kiureghian[52] calculated D_p using Eqs. (2) and (3) together with Eq. (4) by Abrahamson[10].

$$\ln(D) = 1.15Mw - 2.83 \qquad (4)$$

Equations (2) to (4) are applied to the 2000 Tottori-ken Seibu earthquake and the 2016 Kumamoto earthquake as shown in Figs. 9(a) and (b). Since both earthquakes are composed of several faults, the fault width W is calculated by weighted average with M_0 of each fault. The values of W are 9.5 km for the 2000 Tottori-ken Seibu earthquake and 11.2 km for the Kumamoto earthquake. Crustal deformation by GNSS[9),49),50] is also shown in Fig. 9. The value of $2x/L$ is shown with different colors in Fig. 9(a). Since the equations are for the infinite vertical strike-slip faults, data in $2x/L < 0$ are excluded. The R_x–D_p prediction equation is consistent to data at TTRH02B and KASHOU, but overestimates data in $|R_x| > 5$ km. In Fig.9 (b) D_p of the prediction equation is calculated assuming $Z_{TOR} = 0$ km for the Futagawa fault near Nishihara and $Z_{TOR} = 0.4$ km for the southern fault, the Hinagu fault based on the fault model by Ozawa et al.[51]. Data on the Hinagu fault zone and the Futagawa fault zone are separately shown. Data on the Hinagu fault zone roughly fit to the equation with $Z_{TOR} = 0.4$ km. This result suggests that the parameter of Z_{TOR} is effective to predict D_p. On the other hand, the equation with $Z_{TOR} = 0$ km underestimates data in $R_x < 5$ km on the Futagawa fault zone.

Figure 10 compares D_p–R_{rup} relations without Z_{TOR} as a parameter with data of the 2016

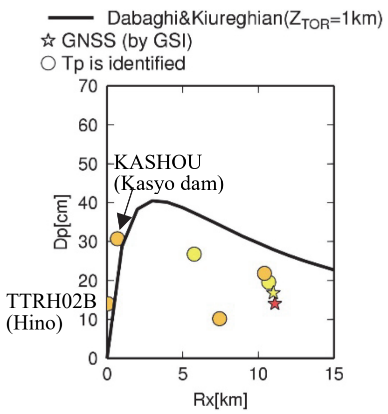

(a) 2000 Tottori-ken Seibu earthquake

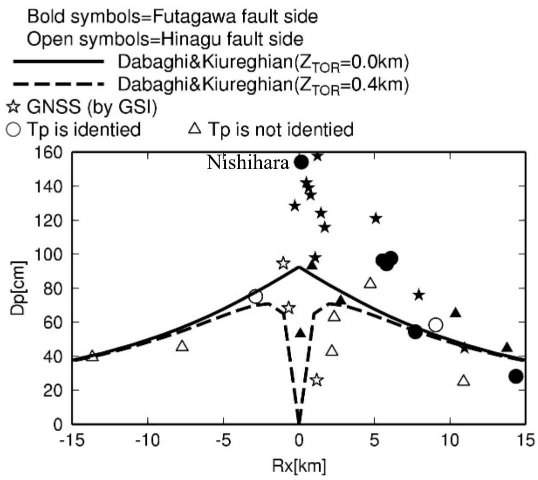

(b) 2016 Kumamoto earthquake

Fig. 9 Relation between R_x and D_p estimated from strong motions, GNSS and previous prediction equations for the strike-slip earthquake

Kumamoto earthquake and the other two surface rupture earthquakes. The prediction equation of D_{p} of the horizontal component by Burks and Baker[13] is shown in Eq. (5).

$$\ln D_{\mathrm{p}} = \ln\left[\frac{2}{\pi} - \tan^{-1}\left(0.3R_{rup}\right)\right] + 1.3M\mathrm{w} - 1.5 \tag{5}$$

where the term of $\tan^{-1}$ is modelled based on Byerly and DeNoyer[14]. The prediction equation of D_{p} of the Fling-P component by Kamai et al.[12] is shown in Eqs. (6) to (8).

$$\ln\left(\frac{D_{\mathrm{p}}}{D}\right) = \ln\left(a_0 + a_4\right) + a_2 \ln\left(\frac{R_{rup} + a_3}{a_3}\right) \tag{6}$$

$$D = \frac{10^{1.5M\mathrm{w}+16.05}}{3\times 10^{11} LW} \qquad \text{for } L \text{ and } W \text{ are known} \tag{7}$$

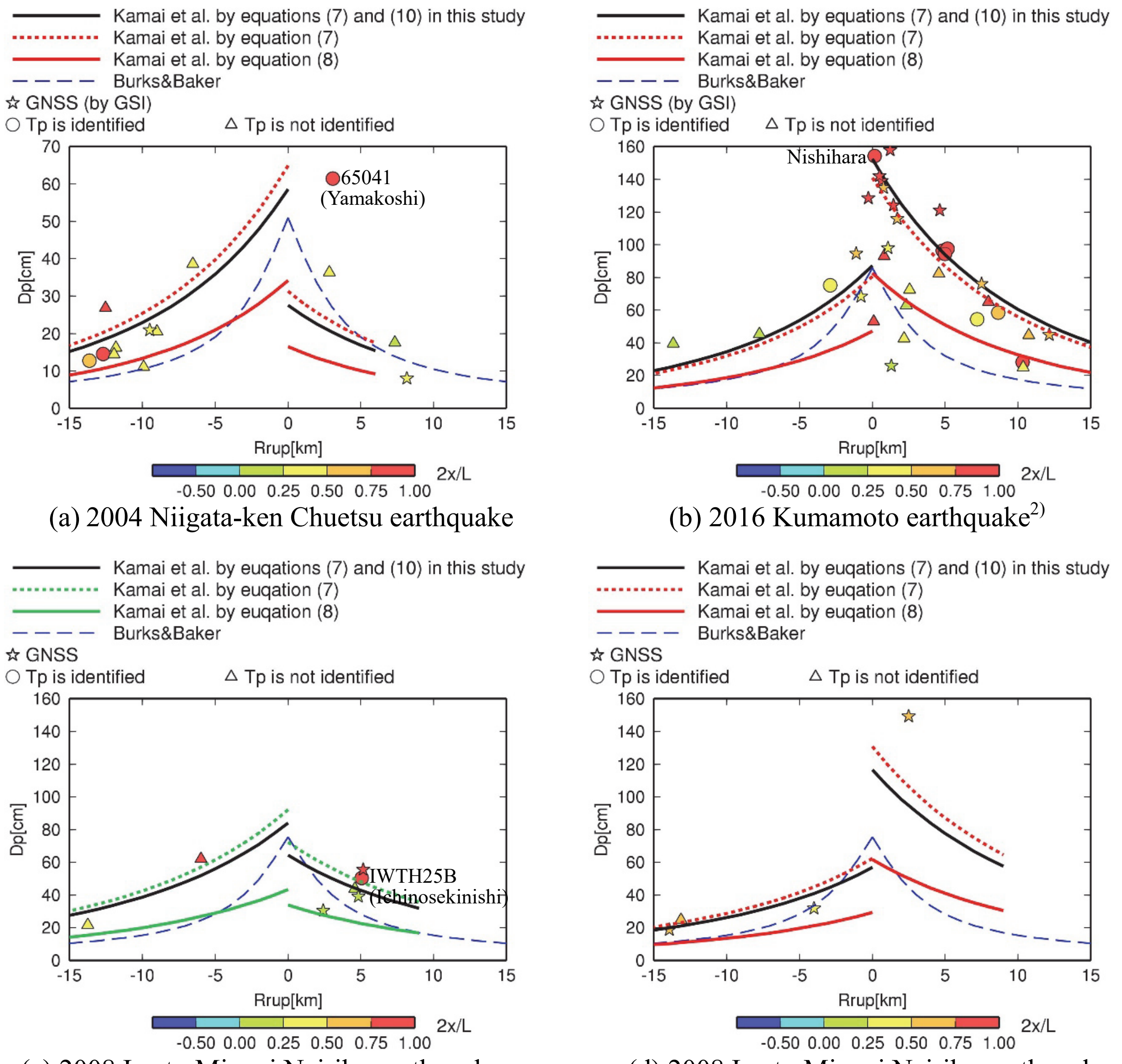

(a) 2004 Niigata-ken Chuetsu earthquake

(b) 2016 Kumamoto earthquake[2]

(c) 2008 Iwate-Miyagi Nairiku earthquake (Northern fault side)

(d) 2008 Iwate-Miyagi Nairiku earthquake (Southern fault side)

Fig. 10 Relation between R_{rup} and D_{p} estimated from strong motions, GNSS and previous prediction equations

$$\ln(D) = 1.15Mw - 3.28 \tag{8}$$

where LW is rupture area S. Eq. (7) is rewritten by substituting $\mu = 3 \times 10^{11}$ dyne/cm^2 into $M_0 = \mu DS$. The a_0, a_2, a_3, and a_4 are constants or values obtained from regression relations with Mw and dip angle as parameters for the Fling-P component of strike-slip faults and the Fling-P and vertical components of reverse faults. For the Fling-P component of reverse faults, only hanging-wall stations on the surface projection of the rupture plane were used in the regression. The equation of $\log_{10}S = M\mathrm{w} - 4$ by Wells and Coppersmith[19] was substituted into Eqs. (5) and (8), both of which were proposed using the same data for the regression relations of T_p mentioned before. In Fig. 10, the relation substituted Eq. (10) which is the M_0–S relation developed in this study as shown later into Eq. (7) is also shown. The dip angles shown in Table 1 are used in the regression relation except for the 2008 Iwate-Miyagi Nairiku earthquake. We use a 30° dip instead of a 25° dip[23] of the southern fault of the 2008 Iwate-Miyagi Nairiku earthquake, because it is impossible to calculate the equation by Kamai et al.[12] for the 25° dip. Data and regression relations of the 2008 Iwate-Miyagi Nairiku earthquake are plotted in Figs. 10(c) and (d) for the northern fault and the southern fault, respectively. Data by GNSS[9),23),49),50] are shown and data with $2x/L < 0$ are excluded in Fig. 10.

We discuss the relation between observed D_p and the prediction equations in Fig. 10. The equation by Kamai et al.[12] substituting Eq. (7) or Eq. (10) into Eq. (6) almost fit to the observed D_p. The other equations underestimate the observed D_p. All prediction equations in Fig. 10 tend to overestimate several data in the near-fault region of the 2016 Kumamoto earthquake, but most of them are on the Hinagu fault zone as shown in Fig. 9(b). This result suggests that the overestimation will be improved by using Z_{TOR} as one of parameters to D_p equations. D_p estimated from strong motion records is the largest at Nishihara during the 2016 Kumamoto earthquake. D_p by GNSS near $R_x = 0$ km during the 2016 Kumamoto earthquake and the 2008 Iwate-Miyagi Nairiku earthquake is the same level to D_p at Nishihara. For the 2004 Niigata-ken Chuetsu earthquake D_p at 65041 (Yamakoshi) is the largest and the prediction equation underestimates it very much if 65041 (Yamakoshi) is assumed to be on the hanging-wall side. However, the prediction equation almost agrees with it if 65041 (Yamakoshi) is assumed to be on the foot-wall side based on the fault model[53] estimated from RADARSAT/InSAR. For the 2008 Iwate-Miyagi Nairiku earthquake the largest D_p is observed on the southern reverse fault with a low dip angle and D_p at IWTH25B (Ichinosekinishi) on the northern reverse fault with a 44.9° dip is relatively small, 52 cm.

The larger $2x/L$ is, the larger D_p is as pointed out[2] from data of the 2016 Kumamoto earthquake. In other words, D_p is large near the center of rupture length. Surface rupture displacements based on field measurements showed the similar results[54] and empirical relations[55] between the surface rupture displacement and x/L were developed. Therefore x/L will be a proper parameter to develop the prediction equation in the feature.

For the 2011 Fukushima-ken Hamadori earthquake D_p of the Fling-P component is observed at three stations shown in Fig. 1(f), but no prediction equations for normal-slip faults have not been proposed. For the 2014 Nagano-ken Hokubu earthquake, the equation by Kamai et al.[12] substituting Eq. (7) or Eq. (10) into Eq. (6) almost fit to $D_\mathrm{p} = 27$ cm at NGN005 (Hakuba). On the other hand, the equation by Kamai et al.[12] substituting Eq. (8) into Eq. (6) underestimates the observed D_p.

Figure 11 compares D_p–R_{rup} relations of prediction equations for vertical component with data of two reverse faults, the 2004 Niigata-ken Chuetsu earthquake and the 2008 Iwate-Miyagi earthquake. D_p at IWTH25B (Ichinosekinishi) and two GNSS stations are larger than D_p of vertical component at Nishihara of the 2016 the Kumamoto earthquake[2] and the prediction equation by Kamai et al.[12]. However, data is insufficient to get systematic features. Since simulated D_p by Ohta et al.[23] underestimated D_p observed at two GNSS stations, that is, a station near IWTH25B and a station with the largest D_p, the equation by Kamai et al.[12] using the fault model by Ohta et al.[23] is thought to underestimate the data. Although trampoline effects[3] or uplifting effects of the observation house due to rocking[56] at a surface station of IWTH25 have been pointed out, the displacement time history of the vertical component at IWTH25B was almost same with that the surface station of IWTH25. The difference of D_p between IWTH25 and IWTH25B was less than 10%[4]. Since the difference of D_p of the vertical component at IWTH25 used[4] in this study is 1 cm from that estimated by Aoi et al.[3], D_p

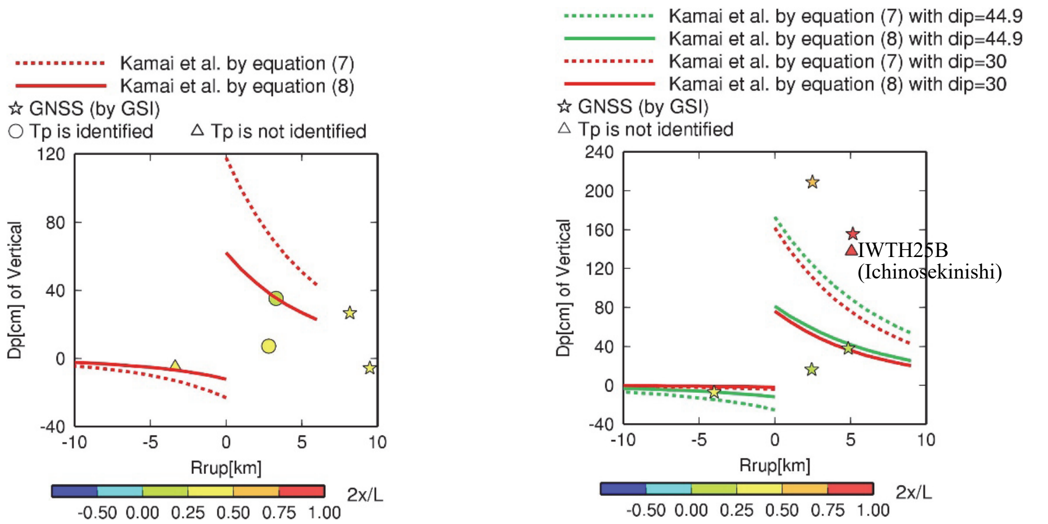

(a) 2004 Niigata-ken Chuetsu earthquake (b) 2008 Iwate-Miyagi Nairiku earthquake

Fig. 11 Relation between R_{rup} and D_p estimated from strong motion records, GNSS and previous prediction equations for vertical component of reverse earthquakes

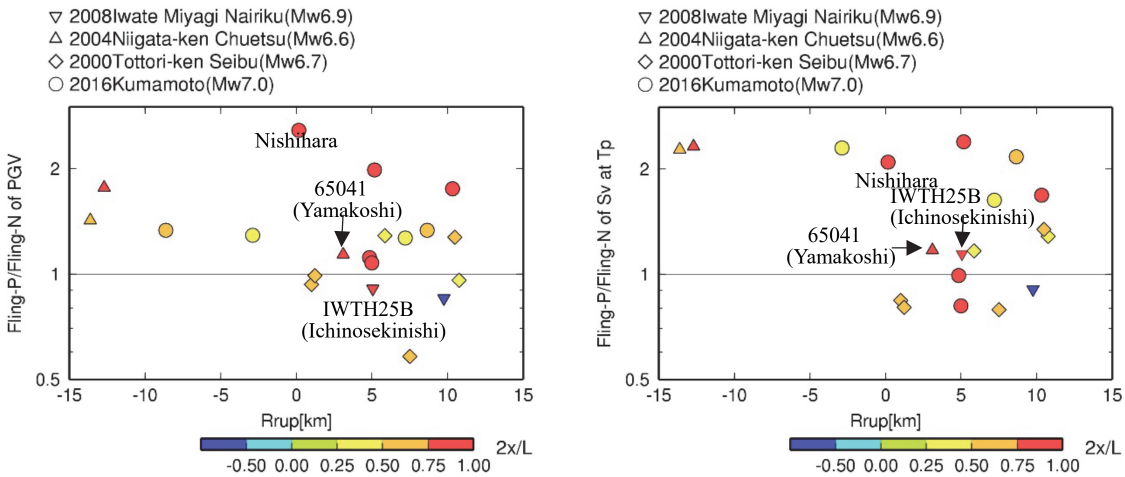

(a) PGV ratios (b) Sv (h = 5%) ratios at T_p

Fig. 12 PGV ratios and Sv ratios at T_p of Fling-P to Fling-N components

estimated at IWTH25B is reliable.

PGV ratios of Fling-P to Fling-N components are examined. Figure 12(a) shows the ratios at stations where T_p is estimated for the 2016 Kumamoto earthquake and the three earthquakes analyzed in this study. R_{rup} adding the same sign to R_x is used in this figure, because R_{rup} is usually used in PGV prediction equations. The PGV ratio at Nishihara with R_{rup} of nearly zero is more than 2.5, which is largest among all. Except for data of the 2016 Kumamoto earthquake, the ratios at two stations with $R_{rup} = -15$ km on the foot-wall side of the 2004 Niigata-ken Chuetsu earthquake are relatively large, but the absolute PGVs are small, that is, less than 20 cm/s. In Fig. 12(b), Sv ratio at T_p is shown. Sv ratios at five stations including Nishihara in about $|R_{rup}| < 10$ km of the 2016 Kumamoto earthquake are large, about two. Although the PGV of the Fling-P component at Nishihara was extremely large, 277 cm/s, the Sv ratio at Nishihara is the same level to the ratios at the other four stations. This is interpreted that the large PGV at Nishihara is greatly influenced by different effects from fling-step. Satoh[2] pointed out that the PGV of the vertical component at Nishihara was explained only by the fling-step, but that of Fling-P component was not.

5. DISCUSSIONS

In order to examine causes the underestimation of D_p by Eqs. (6) and (8) by Kamai et al.[12], Fig. 13 shows M_0–S and M_0–D relations of fault models from geodetic data and strong motions records shown in Table 2 and previous equations. Table 2 shows M_0, S, and D of fault models from geodetic data together with references of fault models from geodetic data and strong motion records. S of fault models from strong motion records was trimmed by the criteria by Somerville et al.[58] except for S for the 2014 Nagano-ken Hokubu earthquake. The M_0–S relation by Wells and Coppersmith[19] is obtained from $\log_{10}S = M\mathrm{w} - 4$, which is used in Kamai et al.[12] M_0–D equations are original relations by Wells and Coppersmith[19], Somerville et al.[58], and Takemura[57] and the relations substituting μ = 3 × 10^{11} dyne/cm^2 into the M_0–S relations by Wells and Coppersmith[19] and Irikura and Miyake[17]. In Kamai et al.[12], D is calculated by substituting μ = 3 × 10^{11} dyne/cm^2 into the M_0–S relation by Wells and Coppersmith[19]. It is found from Fig. 13 that S from geodetic data is smaller than S from strong motion records and that D from geodetic data is larger than D from strong motion records. S by the M_0–S relation of fault models from geodetic data is smaller than S of the equations by Somerville et al.[58],

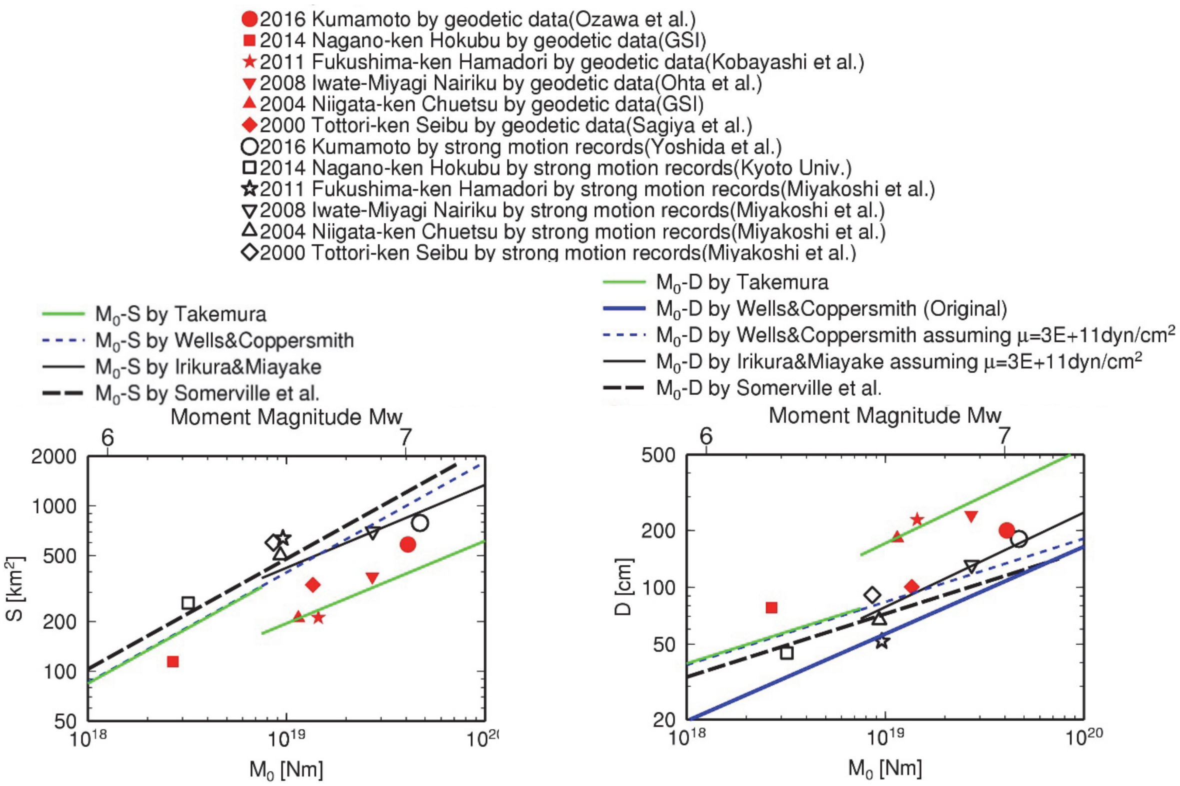

Fig. 13 Comparison between M_0–S and M_0–D relations of fault models from strong motion records and geodetic data and previous prediction equations[17),19),57),58]

Table 2 Fault parameters of earthquakes used for the study on D_p and T_p

Event	Fault Models from Geodetic Data						Fault Models from Strong Motion Records
	S[km^2]	M$_0$[Nm]	D[m]	Reference	Data	Remarks	
2000 Tottori-ken Seibu earthquake	333.2	1.36E+19	1.00	21)	GNSS, Leveling	Heterogeneous Slip	59)
2004 Niigata-ken Chuetsu earthquake	210.1	1.15E+19	1.82	22)	GNSS	Homogeneous Slip	59)
2008 iwate-Miyagi Nairiku earthquake	375.0	2.70E+19	2.40	23)	GNSS	Homogeneous Slip	59)
2011 Fukushima-ken Hamadori earthquake	211.9	1.45E+19	2.28	24)	InSAR	Homogeneous Slip	59)
2014 Nagano-ken Hokubu earthquake	114.6	2.68E+18	0.78	25)	GNSS	Homogeneous Slip	60)
2016 Kumamoto earthquake	587.7	4.10E+19	2.00	51)	GNSS	Homogeneous Slip	61)

Irikura and Miyake[17)] and Wells and Coppersmith[19)] and is larger than S of the equation by Takemura[57)]. Strong motions in Burks and Baker[13)] and Kamai et al.[12)] were predicted assuming fault models based on the M_0–S relation by Wells and Coppersmith[19)] and so it is thought that D is underestimated. Resultantly, D_p which is proportional to D is underestimated.

We examine if the difference of M_0–S relations of fault models from geodetic data and strong motion records is the same that of the other crustal earthquakes in Japan. Figure 14 shows M_0–S and M_0–D relations in this study from fault models shown in Tables 2 and 3[62)–71)] and previous M_0–S and M_0–D equations. For fault models of the 2007 Niigata-ken Chuetsu-oki earthquake by Geospatial Information Authority of Japan[41)], both a heterogeneous-slip model and the trimmed model with final slip larger than 1 m are shown assuming $\mu = 3 \times 10^{11}$ dyne/cm^2. The earthquakes with the same M_0 range to the equation by Irikura and Miyake[17)] are used, since D with smaller M_0 is smaller. The M_0–S relation of the fault models from strong motion records shown in Table 3 was pointed out[59)] to almost agree with the equation by Irikura and Miyake[17)]. Since area with small amount of slip are included in S for heterogeneous-slip models from geodetic data, S of the heterogeneous-slip models tend to be

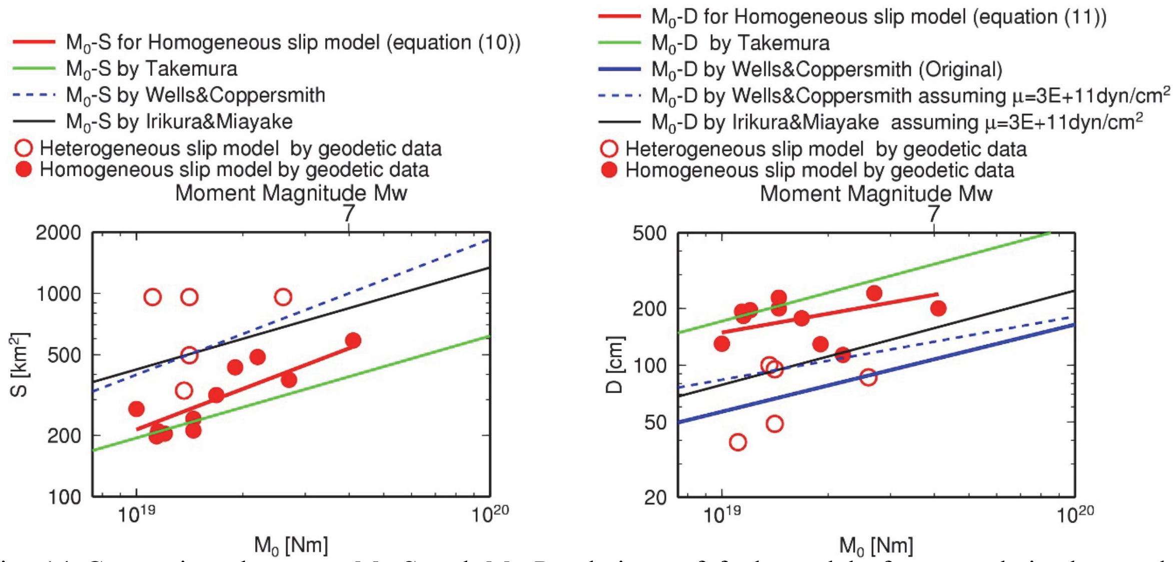

Fig. 14 Comparison between M_0–S and M_0–D relations of fault models from geodetic data and previous prediction equations[17),19),57),58)]

Table 3 Fault parameters from geodetic data of earthquakes added for study on scaling relations

Event	Fault Models from Geodetic Data					
	S[km^2]	M_0[Nm]	D[m]	Reference	Data	Remarks
1995 Hyogo-ken Nanbu earthquake	486.9	2.20E+19	1.13	62)	GNSS, Leveling	Homogeneous Slip
	960.0	2.60E+19	0.86	63)	GNSS, Leveling, Triangulation	Heterogeneous Slip, Horizontaly Layered Media
	432.5	1.90E+19	1.29	64)	GNSS, Leveling, Triangulation, InSAR	Homogeneous Slip
2007 Noto Hanto earthquake	269.7	1.00E+19	1.30	65)	GNSS	Homogeneous Slip
	960.0	1.11E+19	0.39	66)	GNSS, InSAR	Heterogeneous Slip
	242.0	1.45E+19	2.00	67)	GNSS, InSAR	Homogeneous Slip
2007 Niigata-ken Chuetsu-oki	316.3	1.68E+19	1.77	68)	GNSS, InSAR	Homogeneous Slip
	198.5	1.14E+19	1.92	69)	GNSS	Homogeneous Slip, Model-2[69)]
	204.9	1.20E+19	1.95	70)	GNSS, Leveling, InSAR	Homogeneous Slip
	960.0	1.41E+19	0.49	71)	GNSS, Leveling, InSAR	Heterogeneous Slip, Horizontaly Layered Media
	498.0	1.41E+19	0.95	71)	GNSS, Leveling, InSAR	Heterogeneous Slip*, Horizontaly Layered Media

* Trimmed fault with final slip larger than about 1 m

larger than those of the homogeneous-slip models. In fact, S of the trimmed model of the 2007 Niigata-ken Chuetsu-oki earthquake is smaller than the original heterogeneous-slip model. S of homogeneous-slip models is less than S of M_0–S relations by Irikura and Miyake[17] and Wells and Coppersmith[19]. D of homogeneous-slip models is less than D by Irikura and Miyake[17] and Wells and Coppersmith[19].

The M_0–S regression relation of homogeneous-slip models is given by Eq. (9).

$$\log_{10}S = -12.71 + 0.79\log_{10}M_0 \tag{9}$$

Calculation of t-test confirms that the slope value of 0.79 is significant at a 95% probability level and that the reliable range is 0.79 ± 0.33. Therefore, it is not determined from this result whether $S \propto M_0^{1/2}$ or $S \propto M_0^{2/3}$ is valid. In order to compare with the Wells and Coppersmith[19] M_0–S equation, the regression relation is calculated assuming $S \propto M_0^{2/3}$.

$$\log_{10}S = -10.34 + (2/3)\log_{10}M_0 \tag{10}$$

S by Eq. (10) is 0.55 times of S by Wells and Coppersmith[19].

The regression relation of M_0–D of homogeneous-slip models gives the slop value of 0.067, but this is not significant at a 95% probability level. In order to compare with Wells and Coppersmith[19] M_0–D equation, however, the regression relation is calculated assuming $D \propto M_0^{1/3}$.

$$\log_{10}D = -6.16 + (1/3)\log_{10}M_0 \tag{11}$$

D by Eq. (11) is 1.7 times of D calculated by substituting $\mu = 3 \times 10^{11}$ dyne/cm^2 into $\log_{10}S = M\mathrm{w} - 4$ by Wells and Coppersmith[19].

D by substituting Eq. (10) into Eq. (7) by Kamai et al.[12] is larger than D by substituting the Wells and Coppersmith[19] M_0–S equation. As a result, D_p observed during the 2016 Kumamoto earthquake, the 2004 Niigata-ken Chuetsu earthquake and the 2008 Iwate-Miyagi Nairiku earthquake is reasonably predicted by using Eqs. (6), (7) and (10) as shown in Fig. 10. One of the reasons is thought that Wells and Coppersmith[19] data were aftershock distributions, active faults, geodetic data and strong motion records and that some of them are not sensitive to static displacements. Although Irikura and Miyake[17] stated that S from strong motion records almost agree with S from aftershock distributions, active faults and a part of geodetic data, the geodetic data are only one part. It is necessary to examine

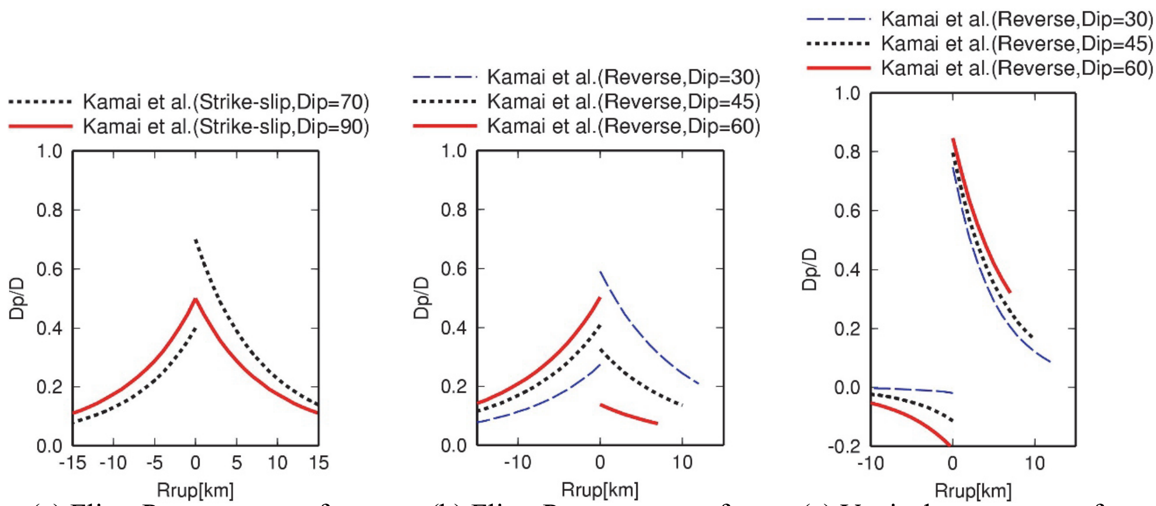

(a) Fling-P component of strike-slip faults (b) Fling-P component of reverse faults (c) Vertical component of reverse faults

Fig. 15 D_p/D for Mw6.7 earthquake calculated by the equation of Kamai et al.[12] developed using synthetics assuming heterogeneous-slip models whether the fact that S from geodetic data is smaller than S from strong motion records is the feature for earthquakes only in Japan in the future.

The effects of dip angles on D_p are discussed. In Fig. 15, D_p/D in M by Kamai et al.[12] is shown for Mw6.7 earthquake with different dip angles. Positive sign of the vertical component indicates uplift. For strike-slip faults, D_p/D of Fling-P component with a 70° dip is larger than that of a 90° dip on the hanging-wall side and the feature on the foot-wall side is reversed. The dip angle of the fault near Nishihara where D_p was the largest during the 2016 Kumamoto earthquake is about 70°[51], which generates larger D_p than a 90° dip. For low-angle reverse faults, D_p/D on the hanging-wall side is larger than that on the foot-wall side. The feature is reversed for high-angle reverse faults. D_p/D on the hanging-wall side for the strike-slip fault with a 70° dip is larger than D_p for the reverse faults. For reverse faults, D_p/D of vertical component does not depend on dip angles so much on the hanging-wall side. On the foot-wall side, D_p/D of vertical component for high-angle reverse faults is larger than that for low-angle reverse faults. Kamai et al.[12] proposed the prediction equations for the reverse fault with a 90° rake and the strike-slip fault with a 180° rake and did not consider the other rake angles.

To show the effects of rake angles on D_p, D_p of the horizontal component is theoretically calculated by Okada's method[44,45]. Mw6.7 fault with L = 30 km and W = 15 km is assumed so that S is nearly equivalent to the M_0–S equation by Irikura and Miyake[17]. Average slip D is 100 cm by assuming S-wave velocity of 3.4 km and density of 2.7 g/cm^3 for the infinite half-space. The top depth is assumed to be 0 km. Figures 16(a) and (b) show results for pure left-lateral strike-slip fault with dip angles of 90° and 70°, respectively. Figures 16(c) shows results for the fault with a 70° dip and a 200° rake, both values are equivalent to the fault[51] near Nishihara. D_p of Fling-P component at NS direction of 0 km and 15 km in Figs. 16(a) to (c) is shown in Figs. 17(a) and (b), respectively. It is confirmed that D_p for the fault with a 70° dip is larger than D_p for the fault with a of 90° dip in near-fault region on hanging-wall side in the case of a 180° rake as shown by the prediction equation by Kamai et al.[12].

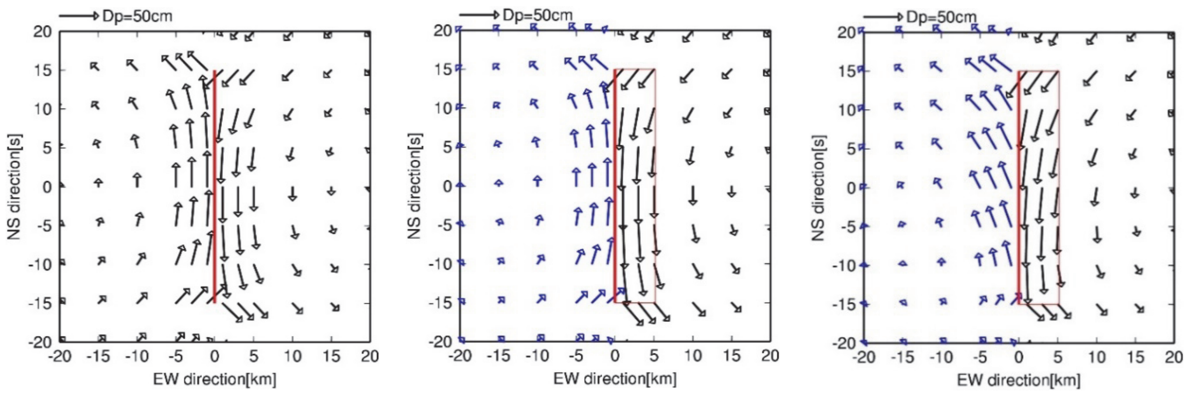

(a) dip = 90°, rake = 180° (b) dip = 70°, rake = 180° (c) dip = 70°, rake = 200°

Fig. 16 D_p distribution of the horizontal component calculated by Okada's method[44,45] using homogeneous-slip models for the Mw6.7 strike-slip earthquake

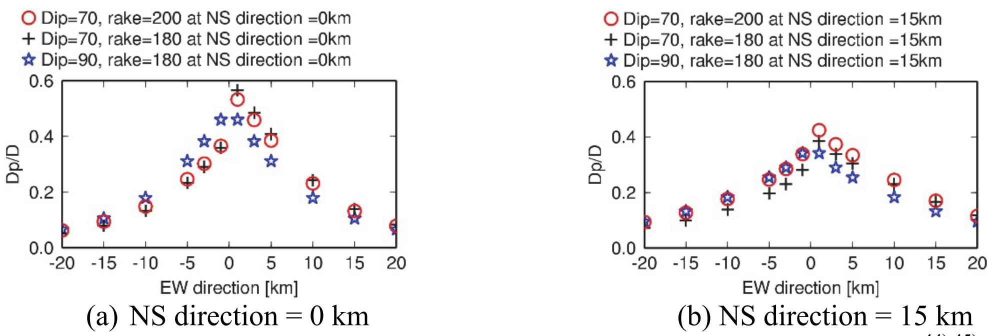

(a) NS direction = 0 km (b) NS direction = 15 km

Fig. 17 D_p/D of the horizontal component calculated by Okada's method[44,45] using homogeneous-slip models for the Mw6.7 strike-slip earthquake

For the fault of with a 70° dip, D_p with a 200° rake is slightly smaller than that with a 180° rake at 0 km of NS direction. In this case, however, D_p on hanging-wall side is larger than D_p on foot-wall side and this is qualitatively consistent with data by GNSS and InSAR in near-fault region close to Nishihara. It is found that Nishihara was located near the center of rupture length where D_p is large in general. For the fault of a 70° dip at 15 km of NS direction, D_p with a 200° rake is larger than that with a 180° rake. In other words, for the fault equivalent to the 2016 Kumamoto earthquake shown in Fig. 16(c), D_p is larger than the other faults at the edge of the fault.

6. CONCLUSIONS

We are aiming at the development of the prediction equations of the static displacement D_p and long-period (2–10 s) velocity pulse using worldwide strong motion records of crustal earthquakes. As the first step, in this study, we extract D_p and the pulse period T_p from strong motion records of crustal earthquakes in Japan and examine them including results of the 2016 Kumamoto earthquake[2]. We select strong motion records of four surface rupture earthquakes and one buried rupture earthquake (the 2000 Tottori-ken Seibu earthquake) from records after the 1995 Hyogo-ken Nanbu earthquake. As a result, D_p is identified from records of all the five earthquakes, but T_p is not identified from records of the 2011 *M*w6.7 Fukushima-ken Hamadori earthquake and *M*w6.2 Nagano-ken Hokubu earthquake. Since the number of vertical components in which long-period pulses are detected is small, results of the Fling-P component, that is, the maximum-direction component of the horizontal vector are summarized as follows.

- T_p of the 2000 *M*w6.7 Tottori-ken Seibu earthquake, the 2004 *M*w6.7 Niigata-ken Chuetsu earthquake, the 2008 *M*w6.9 Iwate-Miyagi Nairiku earthquake and the 2016 *M*w7.0 Kumamoto earthquake is about 3 s in $|R_x| < 12$ km. The estimated T_p is averagely close to the *M*w–T_p relation by Burks and Baker[13]. Since *M*w range of our data is small, *M*w dependency is not so clear.
- D_p near $R_x = 0$ km of the 2000 Tottori-ken Seibu earthquake is explained by a previous prediction equation considering a top depth of the fault Z_{TOR} as a parameter. D_p of the 2004 *M*w6.7 Niigata-ken Chuetsu earthquake, the 2008 *M*w6.9 Iwate-Miyagi Nairiku earthquake as well as the 2016 *M*w7.0 Kumamoto earthquake almost agrees with the prediction equation by Kamai et al.[12] in which *M*w, rupture area *S*, dip angle and rupture distance are used as parameters. On the other hand, the equation by Kamai et al.[12] in which *S* is not used as one of parameters underestimates the observed D_p, and it is thought to be because the M_0–S relation by Wells and Coppersmith[19] is substituted into the equation by Kamai et al.[12]. In other words, *S* from M_0–S relation by Wells and Coppersmith[19] is larger than *S* from the M_0–S relation of fault models from geodetic data for the earthquakes used in this study, and so the average slip *D* in the equation by Kamai et al.[12] becomes smaller.
- We examine the M_0–S relation by adding fault models from geodetic data of the other three crustal earthquakes with *M*w ≥ 6.5 in Japan to the fault models mentioned above. *S* of homogeneous-slip models from geodetic data is smaller than *S* of fault models from strong motion records and the M_0–S relations by Wells and Coppersmith[19] and Irikura and Miyake[17], but is larger than the M_0–S relation by Takemura[57]. We estimate an M_0–S relation using homogeneous-slip models from geodetic data and substitute the relation into D_p prediction equation by Kamai et al.[12]. As a result, D_p of three surface rupture earthquakes is reasonably predicted by the equation, because the average slip becomes larger.
- D_p of three surface rupture earthquakes tends to be large near the center of rupture length as pointed out from D_p of the 2016 Kumamoto earthquake[2]. Prediction equations of D_p will be improved by using this as a parameter.
- The 2016 *M*w7.0 Kumamoto earthquake is the surface-rupture strike-slip earthquake with a 70° dip. These fault parameters are good conditions to generate larger D_p than the vertical strike-slip earthquakes near the fault on the hanging-wall side. The location of Nishihara observed the largest D_p among strong motion records of crustal earthquakes in Japan was the center of the rupture length in the very near-fault on the hanging-wall side. This is also the good condition to generate

large D_p in general.

ACKNOWLEDGMENTS

We use strong motions records by NIED (K-NET and KiK-net), JMA, local governments (Niigata, Iwate, Miyagi and Akita prefectures), NILIM, JSCE (from JR East and NEXCO East) and CEORKA. JMA unified hypocenter catalog and NIED F-net catalog are used. The code by Okada[44] on download site of NIED[45] is used. GMT[72] is used to plot figures.

REFERENCES

1) Iwata, T.: Analysis of Strong Motion Records Observed at Miyazono in Mashiki Town and Komori in Nishihara Village, http://sms.dpri.kyoto-u.ac.jp/topics/masiki-nishihara0428ver2.pdf (in Japanese, last accessed on November 8, 2017)
2) Satoh, T.: Study on Long-Period Pulse and Permanent Displacement of the 2016 Kumamoto Earthquake Based on Comparison with Previous Prediction Equations, *Journal of Structural and Construction Engineering* (Transactions of AIJ), No. 750, pp. 1117‑1127, 2018. (in Japanese)
3) Aoi, S. Kunugi, T., Fujiwara, H., Morikawa, N. and Suzuki, W.: Strong Motions of the 2008 Iwate-Miyagi Nairiku Earthquake －Asymmetric Ground Motion and Trampoline Effect－, *Natural Disaster Research Report of NIED,* Vol. 43, pp. 19–29, 2010. (in Japanese)
4) Satoh, T.: Improvement of Generation Method of Three Components of Statistical Green's Functions Considering Near-Field and Intermediate-Field Terms, *Journal of Structural and Construction Engineering* (Transactions of AIJ), No. 638, pp. 629–638, 2009. (in Japanese)
5) Toda, S., Maruyama, T., Yoshimi, M., Kaneda, H., Awata, Y., Yoshida, T. and Ando, R.: Surface Rupture Associated with the 2008 Iwate-Miyagi Nairiku, Japan, Earthquake and its Implications to the Rupture Process and Evaluation of Active Faults, *Zisin*, Vol. 62, pp. 153–178, 2010. (in Japanese)
6) Suzuki, Y., Watanabe, M. and Hirouchi, D.: Surface Earthquake Fault of the Mid Niigata Prefecture Earthquake in 2004, *Journal of Geography*, Vol. 113, pp. 861–870, 2004. (in Japanese)
7) Mizoguchi K., Uehara and Ueta, K.: Surface Fault Ruptures and Slip Distributions of the Mw6.6 11 April 2011 Hamadoori, Fukushima Prefecture, Northeast Japan, Earthquake, *Bulletin of the Seismological Society of America*,, Vol. 102, pp. 1949–1956, 2012.
8) Ishimura, D., Okada, S., Niwa, Y. and Toda, S.: The Surface Rupture of the 22 November 2014 Nagano-ken-hokubu Earthquake (Mw6.2), Along the Kamishiro Fault, Japan, *Active Fault Research*, Vol. 43, pp. 95‑108, 2015. (in Japanese)
9) Geospatial Information Authority of Japan: : List of Earthquakes Detected Crustal Deformation by GEONET, http://mekira.gsi.go.jp/catalogue/index.html (in Japanese, last accessed on November 1, 2017)
10) Abrahamson, N. A.: Development of Fling Model for Diablo Canyon ISFSI, *Pacific Gas and Electric Company, Geosciences Department*, Calc. No. GEO. DCPP, 1, 2001.
11) Abrahamson, N. A.: Velocity Pulses in Near-fault Ground Motions, *Proceedings of the UC Berkeley-CUREE Symposium in Honor of Ray Clough and Joseph Penzien*: Berkeley, California, UC Berkeley, Consortium of Universities for Research in Earthquake Engineering, pp. 40–41, 2002.
12) Kamai, R., Abrahamson, N. A. and Graves, R. W.: Adding Fling Effects to Processed Ground-Motion Time Histories, *Bulletin of the Seismological Society of America*, pp. 1914–1929, Vol. 104, 2014.
13) ar-fault Ground Motions Based on Recordings and Simulations, *Soil Dynamics and Earthquake* Burks, L. S. and Baker, J. W.: A Predictive Model for Fling-step in Ne*Engineering*, Vol. 80, pp. 119–126, 2016.
14) Byerly, P. and DeNoyer, J.: Energy in Earthquakes as Computed from Geodetic Observations, *in Contributions in Geophysics in Honor of Beno Gutenberg*, Vol. 1, Pergamon Press, pp. 17–35,

1958.
15) Dreger, D., Hurtado, G., Chopra, A. and Larsen, S.: Near-field Across-fault Seismic Ground Motions, *Bulletin of the Seismological Society of America*, Vol. 101, pp. 202–221, 2011.
16) Graves, R. W. and Pitarka, A.: Broadband Ground-motion Simulation Using a Hybrid Approach, *Bulletin of the Seismological Society of America*, Vol. 100, pp. 2095–2123, 2010.
17) Irikura, K. and Miyake, H.: Prediction of Strong Ground Motions for Scenario Earthquakes, *Journal of Geography*, Vol. 110, Issue 6, pp. 849–875, 2001. (in Japanese)
18) The Headquarters for Earthquake Research Promotion: Strong Ground Motion Prediction Method for Earthquakes with Specified Source Faults (“Recipe”), http://www.jishin.go.jp/main/chousa/17_yosokuchizu/recipe.pdf (in Japanese, last accessed on November 8, 2017).
19) Wells, D. L. and Coppersmith, K. J.: New Empirical Relationships Among Magnitude, Rupture Length, Rupture Width, Rupture Area, and Surface Displacement, *Bulletin of the Seismological Society of America*, Vol. 84, pp. 974‐1002, 1994.
20) Irikura, K. and Kurahashi, S.: Extension of Characterized Source Model for Long-Period Strong Motions Near Surface-Rupture-Earthquake, Validation by Near-Field Strong Motions of the 2016 Kumamoto Earthquake, *Proceedings of the 13th Annual Meeting of Japan Association for Earthquake Engineering*, P3–1, 2017. (in Japanese)
21) Sagiya, T., Nishimura, T., Hatanaka, Y., Fukuyama, E. and Ellsworth, L.: Crustal Movements Associated with the 2000 Western Tottori Earthquake and its Fault Models, *Zisin*, Vol. 54, pp. 523–534, 2002. (in Japanese)
22) Geospatial Information Authority of Japan: Crustal Movements in the Hokuriku and Chubu District, *Report of the Coordinating Committee for Earthquake Prediction, Japan*, Vol. 73, pp. 269–303, 2005. (in Japanese)
23) Ohta, Y., Ohzono, M., Miura, S., Iinuma, T., Tachibana, K., Takatsuka, K., Miyao, K., Sato, T. and Umino, N.: Coseismic Fault Model of the 2008 Iwate-Miyagi Nairiku Earthquake Deduced by a Dense GPS Network, *Earth, Planets and Space*, Vol. 60, pp. 1197–1201, 2008.
24) Kobayashi, T., Tobita, M., Koarai, M., Okatani, T., Suzuki, A., Noguchi, Y., Yamanaka, M. and Miyahara, B.: InSAR-derived Crustal Deformation and Fault Models of Normal Faulting Earthquake (Mj 7.0) in the Fukushima-Hamadori Area, *Earth, Planets and Space*, Vol. 64, pp. 1209–1221, 2012.
25) Geospatial Information Authority of Japan: Crustal Movements in the Kanto and Koshinetsu District, *Report of the Coordinating Committee for Earthquake Prediction, Japan*, Vol. 93, pp. 118–124, 2014. (in Japanese)
26) Asano, K. and Iwata, T.: Source Rupture Process of the 2004 Chuetsu, Mid-Niigata Prefecture, Japan, Earthquake Inferred from Waveform Inversion with Dense Strong-Motion Data, *Bulletin of the Seismological Society of America*, Vol. 99, pp. 123–140, 2009.
27) Shiomi, K., Sekine, S., Takeda, T. and Asano, Y.: Contribution to the Hypocenter Determination of Seismic Stations Within the Source Region of the 2008 Iwate-Miyagi Inland Earthquake, *Report of the Coordinating Committee for Earthquake Prediction, Japan*, Vol. 81, pp. 169–171, 2009. (in Japanese)
28) Panayotopoulos, Y., Hirata, N., Hashima, A., Iwasaki, T., Sakai, S. and Sato, H.: Seismological Evidence of an Active Footwall Shortcut Thrust in the Northern Itoigawa-Shizuoka Tectonic Line Derived by the Aftershock Sequence of the 2014 M6.7 Northern Nagano Earthquake, *Tectonophysics*, Vol. 679, pp. 15–28, 2016.
29) Kinoshita, S.: Kyoshin Net (K-NET), *Seismological Research Letters*, Vol. 69, pp. 309–332, 1998.
30) Aoi, S., Kunugi, T. and Fujiwara, H.: Strong-motion Seismograph Network Operated by NIED: K-NET and KiK-net, *Journal of Japan Association for Earthquake Engineering*, Vol. 4, No. 3, pp. 65–74, 2004.
31) Nishimae, Y.: Observation of Seismic Intensity and Strong Ground Motion by Japan Meteorological Agency and Local Governments in Japan, *Journal of Japan Association for Earthquake Engineering*, Vol. 4, No. 3, pp. 75–78, 2004.

32) National Institute for Land, Infrastructure Management, Ministry of Land, Infrastructure, Transport and Tourism, Japan: Seismometers Installed in Dams Under the Jurisdiction of the Ministry of Land, Infrastructure, Transport and Tourism, *TECHNICAL NOTE of National Institute for Land, Infrastructure Management*, Vol. 733, http://www.nilim.go.jp/lab/bcg/siryou/tnn/tnn0733.htm (in Japanese, last accessed on July 25, 2018)
33) National Institute for Land, Infrastructure Management, Ministry of Land, Infrastructure, Transport and Tourism, Japan: Acceleration Records at Dams Under the Jurisdiction of the Ministry of Land, Infrastructure, Transport and Tourism, *TECHNICAL NOTE of National Institute for Land, Infrastructure Management*, Vol. 734, http://www.nilim.go.jp/lab/bcg/siryou/tnn/tnn0734.htm (in Japanese, last accessed on July 25, 2018)
34) Japan Society of Civil Engineers: Download Site of Earthquake Records, http://committees.jsce.or.jp/jsce_download/node/1 (in Japanese, last accessed on May 26, 2020)
35) Fukuyama, E., Ishida, M., Dreger, D. S. and Kawai, H.: Automated Seismic Moment Tensor Determination by Using On-line Broadband Seismic Waveforms, *Zisin*, Vol. 51, pp. 149–156, 1998. (in Japanese)
36) Toki, K., Irikura, K. and Kagawa, T.: Strong Motion Records in the Source Area of the Hyogoken-Nambu Earthquake, January 17, 1995, Japan, *Journal of Natural Disaster Science*, Vol. 16, No. 2, pp. 23–30, 1995.
37) Kagawa, T., Iemura, H., Irikura, K. and Toki, K.: Strong Ground Motion Observation by the Committee of Earthquake Observation and Research in the Kansai Area (CEORKA), *Journal of Japan Association for Earthquake Engineering*, Vol. 4, No. 3, pp. 128–133, 2004.
38) Special Committee of AIJ on the Hyogo-ken Nanbu Earthquake, 1-SWG1 of Special Research Topic: *Strong Motion Records of the 1995 Kyogo-ken Nanbu earthquake*, Earthquake-Resistant Structure Research Subcommittee, AIJ Kinki Branch, pp. 1–265, 1996. (in Japanese)
39) Hashimoto, M., Sagiya, T., Tsuji, H., Hatanaka, Y. and Tada, T.: Co-seismic Displacements of the 1995 Hyogo-ken Nanbu Earthquake, *Journal of Physics of the Earth,* Vol. 44, pp. 255–279, 1996.
40) Zahradník, J. and Plešinger, A.: Long-period Pulses in Broadband Records of Near Earthquakes, *Bulletin of the Seismological Society of America*, Vol. 95, pp. 1928–1939, 2005.
41) Kaklamanos, J., Baise, L. G. and Boore, D. M.: A Framework for Estimating Unknown Input Parameters When Implementing the NGA Ground Motion Prediction Equations in Engineering Practice, *Earthquake Spectra*, Vol. 27, pp. 1219–1235, 2011.
42) Midorikawa, S. and Nogi, Y.: Estimation of V_{S30} from Shallow Velocity Profile, *Journal of Japan Association for Earthquake Engineering,* Vol. 15, No. 2, pp. 91–96, 2015. (in Japanese)
43) Satoh, T.: Scaling Law of Short-Period Source Spectra for Crustal Earthquakes in Japan Considering Style of Faulting of Dip-Slip and Strike-Slip, *Journal of Structural and Construction Engineering* (Transactions of AIJ), No. 651, pp. 923–932, 2010. (in Japanese)
44) Okada, Y.: Internal Deformation due to Shear and Tensile Faults in a Half-Space, *Bulletin of the Seismological Society of America*, Vol. 82, pp. 1018–1040, 1992.
45) National Research Institute for Earth Science and Disaster Resilience: Program to Calculate Deformation due to a Fault Model DC3D0/DC3D, http://www.bosai.go.jp/study/application/dc3d/DC3Dhtml_J.html (last accessed on July 25, 2018)
46) Horikawa, H. Sekiguchi, H., Iwata, T. and Sugiyama, Y.: A Fault Model of the 2000 Tottori-ken Seibu Earthquake, *Annual Report on Active Fault and Paleoearthquake Researches,* No. 1, pp. 27–40, 2001. (in Japanese)
47) Iwata, T. and Sekiguchi, H.: Source Process and Near-Source Ground Motion During the 2000 Tottori-ken Seibu Earthquake, *Proceedings of the 11th Japan Earthquake Engineering Symposium,* pp. 125–128, 2002. (in Japanese)
48) Sakai, K. and Nozu, A.: Characterized Source Model and Strong Ground Motion Simulation for the 2004 Mid Niigata Prefecture (Niigata-ken Chuetsu) Earthquake Based on Empirical Site Amplification and Phase Effect, *Journal of Japan Association for Earthquake Engineering,* Vol. 11, No. 3. pp. 40–58, 2011. (in Japanese)
49) Geospatial Information Authority of Japan: Information of the 2016 Kumamoto Earthquake,

Results of Campaign GNSS Observation, http://www.gsi.go.jp/common/000142617.png (in Japanese, last accessed on November 1, 2017)
50) Ueshiba, H., Miura, Y., Miyahara, B., Nakai, H., Honda, M., Kakiage, Y., Yamashita, T., Yarai, H., Kobayashi , T .and Morishita, Y.: Crustal deformation of the Kumamoto Earthquake Detected by ALOS-2 InSAR Images, *Journal of the Geospatial Information Authority of Japan*, No. 128, pp. 139–146, 2016. (in Japanese)
51) Ozawa, T., Fujita, E. and Ueda, H.: Crustal Deformation Associated with the 2016 Kumamoto Earthquake and Its Effect on the Magma System of Aso Volcano, *Earth, Planets and Space*, Vol. 68: 186, doi:10.1186/s40623-016-0563-5, 2016.
52) Dabaghi, M. and Kiureghian, D. A.: Stochastic Modeling and Simulation of Near-Fault Ground Motions for Performance-Based Earthquake Engineering, *PEER Report*, No. 2014/20, pp. 1–254, 2014.
53) Ozawa, T., Nishimura, S., Wada, Y. and Ohkura, H.: Coseismic Deformation of the Mid-Niigata Prefecture Earthquake in 2004 Detected by RADARSAT/InSAR, *Earth, Planets and Space*, Vol. 57, pp. 423–428, 2005.
54) Biasi, G. P. and Weldon, II, R. J.: Estimating Surface Rupture Length and Magnitude of Paleoearthquakes from Point Measurements of Rupture Displacement, *Bulletin of the Seismological Society of America*, Vol. 96, pp. 1612–1623, 2006.
55) Biasi, G. P., Weldon, II, R. J. and Dawson, T. E.: Appendix F-Distribution of Slip in Ruptures, Uniform California Earthquake Rupture Forecast, Version 3 (UCERF3)—The Time-independent Model, *USGS Open-File Report* 2013-1165, *CGS Special Report* 228, *and Southern California Earthquake Center Publication,* 1792, pp. 1–41, 2013.
56) Ohmachi, T., Inoue, S., Mizuno, K. and Yamada, M.: Estimated Cause of Extreme Acceleration Records at the KiK-net IWTH25 Station During the 2008 Iwate-Miyagi Nairiku Earthquake, Japan, *Journal of Japan Association for Earthquake Engineering*, Vol. 11, No. 1, pp. 32–47, 2011. (in Japanese)
57) Takemura, M.: Scaling Law for Japanese Intraplate Earthquakes in Special Relations to the Surface Faults and the Damages, *Zisin*, Vol. 51, pp. 211–228, 1998. (in Japanese)
58) Somerville, P. G., Irikura, K., Graves, R. W., Sawada, S., Wald, D., Abrahamson, N., Iwasaki, Y., Kagawa, T., Smith, N. and Kowada, A.: Characterizing Crustal Earthquake Slip Models for the Prediction of Strong Ground Motion, *Seismological Research Letters*, Vol. 70, pp. 59–80, 1999.
59) Miyakoshi, K., Irikura, K. and Kamae, K.: Re-Examination of Scaling Relationships of Source Parameters of the Inland Crustal Earthquakes in Japan Based on the Waveform Inversion of Strong Motion Data, *Journal of Japan Association for Earthquake Engineering*, Vol. 15, No. 7, pp. 141–156, 2015. (in Japanese)
60) Disaster Prevention Research Institute Kyoto University: Source Rupture Process of the 2014 Nagano-ken Hokubu Earthquake, http://www.mext.go.jp/b_menu/shingi/gijyutu/gijyutu6/toushin/attach/icsFiles/afieldfile/2017/07/24/1388141_1.pdf (in Japanese, last accessed on July 26, 2018)
61) Yoshida, K., Miyakoshi, K., Somei, K. and Irikura, K.: Source Process of the 2016 Kumamoto Earthquake (Mj7.3) Inferred from Kinematic Inversion of Strong-Motion Records, *Earth, Planets and Space*, Vol. 69: 64, doi:10.1186/s40623-017-0649-8, 2017.
62) Hashimoto, M., Sagiya, T., Tsuji, H., Hatanaka, Y. and Tada, T.: Co-seismic Displacements of the 1995 Hyogo-ken Nanbu Earthquake, *Journal of Physics of the Earth*, Vol. 44, pp. 255–279, 1996.
63) Yoshida, S., Koketsu, K., Shibazaki, B., Sagiya, T., Kato, T. and Yoshida, Y.: Joint Inversion of Near- and Far-field Waveforms and Geodetic Data for the Rupture Process of the 1995 Kobe Earthquake, *Journal of Physics of the Earth*, Vol. 44, pp. 437–454, 1996.
64) Ozawa, S., Murakami, M., Fujiwara, S. and Tobita, M.: Synthetic Aperture Radar Interferogram of the 1995 Kobe Earthquake and Its Geodetic Inversion, *Geophysical Research Letters*, Vol. 24, No. 18, pp. 2327–2330, 1997.
65) Hiramatsu, Y., Moriya, K., Kamiya, T., Kato, M. and Nishimura, T.: Fault Model of the 2007 Noto Hanto Earthquake Estimated from Coseismic Deformation Obtained by the Distribution of Littoral Organisms and GPS: Implication for Neotectonics in the Northwestern Noto Peninsula,

Earth, Planets and Space, Vol. 60, pp. 903–913, 2008.
66) Fukushima, Y., Ozawa, T. and Hashimoto, M.: Fault Model of the 2007 Noto Hanto Earthquake Estimated from PALSAR Radar Interferometry and GPS Data, *Earth, Planets and Space*, Vol. 60, pp. 99–104, 2008.
67) Ozawa, S., Yarai, H., Tobita, M., Une, H. and Nishimura, T.: Crustal Deformation Associated with the Noto Hanto Earthquake in 2007 in Japan, *Earth, Planets and Space*, Vol. 60, pp. 95–98, 2008.
68) Aoki Y., Furuya, M. and Kato, T.: Coseismic Deformation due to the 2007 Chuetsu-oki Earthquake (Mw = 6.8), *Earth, Planets and Space*, Vol. 60, pp. 1075–1080, 2008.
69) Ohta, Y., Miura, S., Iinuma, T., Tachibana, K., Matsushima, T., Takahashi, H., Sagiya, T., Ito, T., Miyazaki, S., Doke, R., Takeuchi, A., Miyao, K., Hirao, A., Maeda, T., Yamaguchi, T., Takada, M., Iwakuni, M., Ochi, T., Meilano, I. and Hasegawa, A.: Coseismic and Postseismic Deformation Related to the 2007 Niigataken Chuetsu-oki Earthquake, *Earth, Planets and Space*, Vol. 60, pp. 1081–1086, 2008.
70) Nishimura T., Tobita, M., Yarai, H., Ozawa, S., Murakami, M., Yutsudo, T., Ishimoto, M., Umesawa, T., Toyofuku, T., Kawamoto, S., Amagai, T., Fujiwara, M., Suzuki, A., Enya, S., Sasaki, T., Yokokawa, M., Oomori, S., Tanoue, S., Ikeda, H., Nemoto, M., Suito, H., Hayashi, F., Une, H., Koarai, M. and Tsuzawa, M.: Crustal Deformation and a Preliminary Fault Model of the 2007 Chuetsu-oki Earthquake Observed by GPS, InSAR, and Leveling, *Earth, Planets and Space*, Vol. 60, pp. 1093–1098, 2008.
71) Geospatial Information Authority of Japan: Crustal Movements in the Hokuriku and Chubu District, *Report of the Coordinating Committee for Earthquake Prediction, Japan*, Vol. 80, pp. 374–411, 2008. (in Japanese)
72) Wessel, P. and Smith, W. H. F.: New, Improved Version of Generic Mapping Tools Released, *EOS Transactions AGU*, Vol. 79, p. 579, 1998.

(Original Japanese Paper Published: November, 2018)
(English Version Submitted: March 23, 2020)
(English Version Accepted: April 20, 2020)